NASA Technical Paper 1168

Correlation of Laser Velocimeter Measurements Over a Wing With Results of Two Prediction Techniques

Danny R. Hoad
Structures Laboratory
U.S. Army R&T Laboratories (AVRADCOM)
Langley Research Center, Hampton, Virginia

James F. Meyers
Langley Research Center
Hampton, Virginia

Warren H. Young, Jr., and Timothy E. Hepner
Structures Laboratory
U.S. Army R&T Laboratories (AVRADCOM)
Langley Research Center, Hampton, Virginia

National Aeronautics
and Space Administration

**Scientific and Technical
Information Office**

1978

SUMMARY

An analytical investigation was conducted using two methods to determine the flow field at the center line of an unswept wing with an aspect ratio of eight. The analysis included a two-dimensional viscous-flow prediction technique for the flow-field calculation and a three-dimensional potential-flow panel method to evaluate the degree of two-dimensionality achieved at the wing center line.

The analysis was intended to provide an acceptable reference for comparison with velocity measurements obtained from a laser velocimeter. These experimental measurement results are presented in NASA TM-74040 and provide a precise detailed definition of the flow near the wing center line.

Good agreement between laser velocimeter measurements and theoretical results indicated that both provided a true representation of the velocity field about the wing at angles of attack of 0.6° and 4.75°. Velocity measurements with the very small wake region indicate a typical velocity defect. However, at an angle of attack of 4.75°, some discrepancies near the surface were found which were probably caused by a short laminar-separation bubble that was not modeled by the theory.

INTRODUCTION

Evaluations of new or improved theoretical or experimental techniques are sometimes difficult due to the complexity of the technique. Quite often the theoretical technique is compared with careful experimental measurements. In many cases, the experimental measurement is so difficult that it is not an accurate measure of the phenomenon analytically modeled. In recent years, significant advancements have been made in analytical techniques. In particular, methods for predicting the two-dimensional unseparated viscous flow over airfoils have become very precise. On the other hand, significant improvements have been made in experimental measurement techniques with the development of the laser velocimeter (LV).

The LV is a nonintrusive fluid-velocity measurement instrument. It has the inherent potential of measuring velocities at which more traditional instruments either cannot physically survive or their presence would compromise the desired measurement. Even with its usefulness so defined, researchers sometimes question the value of the measurements by the LV. In response to these concerns, some investigators performed a detailed error analysis of the LV system including seed-particle size for

accurate response to velocity gradients (refs. 1 and 2). For situations in which the velocity gradients are too great for accurate particle response, the effect of this error should be determined and is discussed in references 3 and 4. The LV measurements are compared with measurements from traditional devices when possible (refs. 5 and 6), however, these comparisons are usually influenced by the presence of the conventional probe.

The LV application in the Langley V/STOL tunnel is planned for measuring the flow field in and near the wake of a rotor system (ref. 7) where other devices cannot accurately make these measurements (refs. 8 to 11). In these situations, it is not possible to provide another measurement or analytical computation with sufficient confidence that can be used as a reference for correlation.

The requirement then exists for such a reference measurement or for a computation obtained in a situation in which the LV technique is the device with the least interference to the flow field. Such investigations have been conducted around simple shapes such as hemispheres and are reported in references 12 and 13. The investigation described in the present paper was designed to provide a correlation with a flow analysis about the midspan of a simple straight wing as the configuration base line. A two-dimensional viscous-flow prediction program, described in reference 14, was chosen as the reference condition and was justified by the fact that this program accurately predicts measured surface pressures, computed from local surface velocities, on a single-element airfoil at low angles of attack. (See ref. 15.) Since a two dimensional investigation could not be conducted, measurements were obtained at the center line of the wing near where two-dimensional flow does exist. To verify this assumption, a three-dimensional potential-flow program (ref. 16) was used as a comparison with the two-dimensional program results.

Recently, a system was installed in the Langley V/STOL tunnel for a short time to measure the flow characteristics over a stalled three-dimensional wing (ref. 1). The system described in this report was similar to that of reference 1. The system was operated in the backscatter mode to facilitate a common platform for transmitting and receiving optics, and for measuring two components of flow velocity. The tunnel flow was seeded with particles of kerosene smoke with a known particle-size distribution output. This seeding is required in order to (1) increase the number of velocity measurements per unit time to minimize tunnel run time; and (2) control measurement precision by providing particles with density and size characteristics which improve tracking fidelity.

SYMBOLS

The axes used for this investigation are presented in figure 1. The units for the physical quantities defined in this paper are in the International System of Units (SI). Although most quantities were measured in this system, some were measured in U.S. Customary Units and converted by using factors given in reference 17.

c wing chord, 0.3048 m

N number of velocity measurements in one ensemble

N_i number of velocity measurements in i^{th} histogram interval as percent of N

U,V local velocity components, direction described by subscript (see fig. 1)

U_R local total velocity, $\sqrt{U^2 \quad V^2}$, m/sec

U_T free-stream velocity determined from pitot-static probe, m/sec

X_c,Y_c coordinate axis relative to wing chord (fig. 1)

X_f,Y_f coordinate axis relative to free stream (fig. 1)

x_c distance downstream from wing leading edge along chord, m

Y_c distance above and perpendicular to wing chord, m

α wing angle of attack, deg

Subscripts:

e ensemble-average data

f direction indication of parameters U, V, X, and Y parallel and perpendicular to free stream (see fig. 1)

i i^{th} measurement in ensemble

L direction indication of velocity components inclined 44.4^o above free stream and 45.6^o below free stream (see fig. 1)

MODEL AND TEST TECHNIQUE

Apparatus

A fringe-type LV optics system operating in the backscatter mode was used for the tests discussed in this report. This system was used to measure two components of velocity inclined 44.4° and -45.6° to a plane parallel to the free stream, and utilized a Bragg cell to eliminate directional ambiguity problems as experienced in reference 1. A sketch of the optics system is presented in figure 2 and a photograph of the system is presented in figure 3. A high-speed burst counter was used to measure the period of the high-frequency signal contained in the burst from the particle traversing the sample volume. LV system control, data acquisition, and data reduction were handled by a minicomputer. A block diagram of the data acquisition system is presented in figure 4. A complete description of the LV optical system, electronics system, and data acquisition and reduction is available in reference 2.

The model used in this investigation was a simple straight wing. It had a span of 2.438 m, a chord of 0.3048 m, and a NACA 0012 airfoil section. Velocity measurements were made at midspan to obtain two-dimensional characteristics. The wing was supported by struts from the floor near the tunnel center line and no balance measurements were taken. The location of the strut mount to the wing was chosen as far outboard as structurally feasible. This provided ample space between struts to minimize flow disturbance at the wing center line. A photograph of the model with crossing laser beams is presented in figure 5.

Local flow velocities were measured about the wing center line at two angles of attack, 0.6° and 4.75°, to compare with theoretical predictions. A pitot-static probe was mounted 2.5 m below and 1 m ahead of the wing center line to provide accurate reference of the free-stream tunnel dynamic pressure. A hygrometer was used to obtain wet-bulb temperatures; the total temperature was measured in the settling chamber. Thus, the tunnel air density could be calculated and, with dynamic pressure measurements, the tunnel velocity could be accurately calculated.

Tunnel Seeding

Perhaps the foremost problem in achieving LV measurement accuracy is particle lag. In most applications, the gas velocity distribution is desired; however, the LV measures the velocity of seed particles in the gas. In many cases, these velocities are identical; however, in regions of

large velocity gradients, such as along a stagnation streamline, the inertia of larger particles does not allow them to adjust immediately to local flow velocity. Care is taken to ensure that the particles within the flow are small enough to follow the flow accurately. This problem was addressed in the investigation described in reference 1. It was found that 3-μm particles responded to the severe velocity gradient (1540 m/sec per meter) along the stagnation line of a hemisphere at a Mach number of 0.55.

Using this LV system, it was determined from laboratory tests and preliminary calculations that, at the focal lengths used in this investigation, the minimum particle size for reasonable signal intensity was on the order of 2 μm . This then put a 2- to 4-μm restriction on the particle size required for practical use of the LV in the Langley V/STOL tunnel.

The smoke generator normally used in the V/STOL tunnel for flow visualization was modified to yield the appropriate particle-size distribution for this test. This distribution was measured by an optical technique similar to that discussed in reference 1 and is presented in figure 6(a). The smoke generator vaporized liquid kerosene by adding heat and emitted a dense white smoke through a nozzle. The nozzle was positioned in the settling chamber of the tunnel to minimize flow disturbance on the model. The nozzle position was critical in that the particles were intended to be only in the area of the measurement volume. The smoke plume in the test section was about 0.4 m in diameter. Any extensive movement of the sample volume resulted in its traversing out of the smoke plume; thus, the nozzle had to be repositioned. This was done manually and was very time-consuming, requiring 20 to 60 min.

DATA ACQUISITION AND REDUCTION

Laser Velocimeter Data Processing

Statistical quantities.- The LV measures velocity events that are Poisson distributed in time at a location in the flow. During the measurement process, two assumptions are made. First, the particles embedded in the flow are not only randomly dispersed in space but are also randomly dispersed in the velocity field; and second, the measurement sample taken over a finite period of time is a good representation of the stationary condition at the measurement location. The statistical quantities of sample mean and standard deviation (and their statistical uncertainties), skew, and excess were computed. Graphical representations of the velocity probability

density functions for each of the velocity components were made by placing each time-history sample of velocity measurements (ensemble) in histogram form and are presented in reference 2.

The sample mean was calculated by three different methods: (1) arithmetic mean, (2) arithmetic mean with corrections for velocity bias and Bragg cell bias (ref. 2), and (3) time averaging (ref. 18). An analysis of these methods is presented in reference 2. It was found in this investigation that the three methods yielded similar results when the mean data rate was above 10 particles per second. (See tables 2 to 4 in ref. 2.) Thus, the statistical mean calculated from the test data was determined by using the simple equation

$$V_e = \frac{V_i}{N}$$

Instrument precision.- The overall measurement precision was obtained by determining the accuracies of all variables in the system which would affect the accuracy of each velocity measurement. Reference 1 provides a complete description of the type of errors involved in this investigation and of the error analysis method.

These errors yield an effective total bias error of -1.33 percent to 0.91percent in velocity calculated by an algebraic sum of the partial bias errors. The total effect of random error was ±0.47 percent uncertainty, which was obtained by taking the square root of the sum of the squares of the partial random errors described in reference 2.

In large velocity gradients, velocity measurement errors may occur if the measurement point is not at the desired location. The two-component mechanical traversing system had a placement uncertainty of ±1 mm, which yielded a worst case (based on the measured velocity flow field) uncertainty in velocity of 1.6percent due to position.

Particle Lag

Since the LV measures particle velocities and not the gas velocity, the final measurement accuracy is dependent on the ability of the particle to follow the flow faithfully. The size distribution of the seed particle was measured with an optical particle-size analyzer which was placed in the test section to capture particles from the generator which yielded acceptable LV signals. The resulting distribution is shown in figure 6(a). The particle size necessary for the LV to obtain valid measurements was determined by using the computer simulation of the

LV developed by Meyers (ref. 19). The probability of a successful measurement (ref. 2) as a function of particle size is shown in figure 6(b). Thus, the overall measurement probability for this test was found (fig. 6 (c)). It was determined from reference 1 that a 3-μm particle traveling at a free-stream Mach number of 0.55 would faithfully follow a velocity gradient of 1540 m/sec per meter. Since this velocity gradient is far greater than any obtained in the present tests, it is concluded that the velocity measurements obtained in this investigation are a true representation of the gas velocity flow field.

TEST AND PROCEDURES

This investigation was conducted in the Langley V/STOL tunnel at a nominal free-stream Mach number of 0.15. The Reynolds number based on the wing chord was approximately 1×10^6. Free-stream measurements were made with the tunnel clear except for the pitot-static probe which was used as a reference. These measurements were made in the vicinity where the model would be positioned. The wing was installed at two angles of attack, 0.6° and 4.75°.

The scan capability of this particular prototype LV system was not sufficient to survey above, ahead of, and behind the wing without moving either the wing or the LV system platform. There was no survey behind the wing at 0.6° angle of attack. With the wing at 4.75° angle of attack, a complete survey was made. To obtain the measurements behind the trailing edge, the model was moved forward and raised inside the test section with very little change to the LV system platform.

To obtain measurements very near the leading edge and trailing edge of the model, the optical center line was inclined off-perpendicular to the tunnel such that the beam nearest the leading (or trailing) edge was aligned with the edge. Thus, the angle of inclination of the optical center line to the wing span was approximately 3° and parallel to the tunnel floor.

DISCUSSION

As mentioned previously, all the velocity measurements at each measurement location were first reduced to histogram form. These histograms are presented in reference 2 with a figure list and a short discussion of interpretation. Statistical analysis of the data was performed as described previously, and the results are presented in tabulated form in reference 2.

Free-Stream Data

Preliminary analysis indicated that, at the Mach number used for this test, the average flow angularity in the tunnel was 0.6° (inclined above tunnel center line). The $U_{f,e}$ and $V_{f,e}$ velocities presented in this paper are, therefore, referenced to free stream rather than tunnel center line. The freestream velocity computed from measurements by the pitot-static probe U_T was used to nondimensionalize these velocity components. Free-stream measurement comparison with the local total velocity U_R indicated errors comparable to the combined pitot-static probe and LV instrument error.

Basic Velocity Data for Wing at $\alpha = 4.75°$ and 0.6°

Details of the statistical characteristics of the velocity data can be found in reference 2. Some of these are summarized herein in the form of contour plots generated by using spline-fit routines between data points. These contour plots are presented in figures 7 to 10 for the wing at $\alpha = 4.75°$ and figures 11 to 14 for the wing at $\alpha = 0.6°$. The "arrow" plots (figs. 7 and 11) indicate the relative location of the velocity measurements and the magnitude and angle of the velocity vector. These plots, of course, were the matrix of data points used to generate the contour plots. These arrow plots indicate the flow field to be what one would expect about an airfoil at low angle of attack. The wake region is definitely evident when $\alpha = 4.75°$. The measurements near the leading edge at $\alpha = 4.75°$ indicate an unexpected phenomenon. This phenomenon is discussed subsequently.

Streamlines (figs. 8 and 12) were generated by allowing a simulated particle to progress through the velocity-field matrix that was generated. The simulated particle responded to the velocity field as it traversed the field. The path of the particle was stored and plotted on-line as a computed streamline. The phenomenon near the leading edge of the wing at $\alpha = 4.75°$ is reflected in the streamline plots. Except for this, these plots are what one would expect to observe using conventional flow-visualization techniques. Local flow angles presented in this manner (figs. 9 and 13) indicate consistent and reasonable characteristics, except for the noted abnormality in the leading-edge region at $\alpha = 4.75°$. Large local flow angles near the crest of the airfoil (25° at $\alpha = 4.75°$ and 17° at $\alpha = 0.6°$) were expected. The flow approaches an angle tangent to the surface at the trailing edge. The contours of constant U_R/U_T indicate the velocity decrease ahead of the airfoil, an increase in velocity over the airfoil, and for the wing at $\alpha = 4.75°$, a wake region with approximately 70 percent of the free-stream velocity,

Prediction Techniques

The external forces generated on a body in a fluid are manifested in the velocity distribution of the fluid about the body. Accurate prediction of this velocity distribution can provide the researcher with a diagnostic tool in interpreting the results of more restrictive measurement techniques. In developing such a prediction technique, a researcher verifies the prediction on the surface of the body with conventional pressure measurements and force measurements. This has been accomplished for the two-dimensional viscous-flow prediction program and is reported in reference 15. Since the local surface pressures are computed from predicted local surface velocities, the off-body velocity prediction should be a very accurate measure of the flow phenomena as measured by the LV. The acceptability of the prediction technique as a reference for the LV measurements is justified by the very accurate agreement with surface pressure measurements.

The theory for the two-dimensional viscous-flow prediction technique is well defined in reference 14 and will be described only in general herein. It involves an iterative procedure which first obtains an inviscid-flow solution for the basic airfoil. A boundary-layer solution is computed based on the inviscid-flow solution, and a modified airfoil is then constructed by adding the boundary-layer displacement thickness to the original airfoil. The inviscid solution for the modified airfoil is obtained and the steps are then repeated until appropriate convergence criteria are satisfied.

Since the wing in this case is not two-dimensional, a three-dimensional flow program was used to determine the effect of three-dimensionality at the center line of the wing. The prediction technique used for this step is an inviscid-flow prediction program and is described in reference 16. This method uses finite-strength vorticity distributions instead of concentrated-line vorticity on the body as is used by other current methods. In this case, the wing was modeled by 160 panels.

Comparison of Experiment With Theory

The two LV-measured components of velocity rotated to the free-stream coordinate system X_f, Y_f are presented in figures 15 to 33 for the wing at $\alpha = 4.75^\circ$ and in figures 34 to 45 for the wing at $\alpha = 0.6^\circ$. Each figure corresponds to a scan perpendicular to the wing chord and can be coupled with the statistical characteristics plots and the histograms in reference 2. The calculated velocities from the two prediction techniques are presented in each figure for comparison with experiment. The three-dimensional predicted velocities agree with the

two-dimensional predicted velocities within 2 percent except very near the airfoil surface. Thus, the assumption of two dimensionality at the center line of the wing is justified.

The theoretical predictions agree well with the LV-measured velocities for the wing at $\alpha = 0.6^{\circ}$. The prediction technique is excellent above the wing and downstream of $x_c/c = 0.08$ (figs. 40 to 45). However, near the leading edge and near the surface of the wing (fig. 37), the predicted velocities are higher than the velocity field. Ahead of the wing (figs. 34 to 36), the prediction techniques provide a reasonably accurate assessment of the velocity field.

With the wing at $\alpha = 4.75^{\circ}$, the prediction agrees only with the velocity measurements away from the surface and the leading edge. At $x_c/c = -0.08$ and -0.04 (figs. 16 and 17), the agreement is good until the measurement location approaches the leading edge. At the leading edge (fig. 18) the predicted velocities are higher than the measured velocities, and this discrepancy continues near the wing surface, at least in the $U_{f,e}$ velocity component, to chord position $x_c/c = 0.13$ (figs. 19 to 23). The $V_{f,e}$ velocity component is underestimated near the surface to chord position $x_c/c = 0.17$ (figs. 19 to 24). The experimental and theoretical velocity values are in good agreement farther aft of this chord position, except in the wake region, since the theory is inadequate in this region. (See figs. 30 to 33.) The wake profile is well defined with the LV. The thickness of the wake is approximately 1.3 mm, which is much too small for conventional probes to measure without altering the characteristics of the wake.

The comparison of experiment and theory in this paper has been shown to be quite good except near the surface of the leading edge for the wing at $\alpha = 4.75^{\circ}$. This discrepancy is not an inadequacy of the prediction methods, but a phenomenon of flow not modeled by the theory. Reference 2 indicated that double-peaked histograms at this location were evidence of a leading-edge laminar separation bubble. This bubble existed between the leading edge, along the upper surface, and trailing edge at $\alpha = 4.75^{\circ}$.

Samples of the histograms are presented in figures 46 and 47. The histograms are presented with a sketch of the wing cross section in which arrows indicate the position, direction, and relative magnitude of the mean velocity vectors. A run consisted of an ensemble of data acquired at the position desired. The scan, therefore, was a series of runs at various y_c/c positions at a constant chordwise position. The histogram is a graphical representation of the variation of velocity measured over a time period. The histograms are presented with N_i, the percentage of that number of measurements within an incremental

velocity band, as a function of velocity. In all cases, the U_L component is presented on the left and the V_L component on the right. Interpretation of histogram information is provided in appendix B of reference 2.

Figure 46 presents the histograms in a scan in which the prediction techniques agreed with the experimentally determined velocity components. (See fig. 15.) The histograms are well-defined Gaussian-type distributed velocity measurements with slight skew indicating fluctuations in velocity and angle as described in appendix B of reference 2. Figure 47 presents the histograms in a scan in which the double peak appears, for example runs 50 to 52, which indicates the presence of the shear layer. These double-peaked histograms indicate that there are two predominant velocity values. The flow oscillates between the two values and shows a tendency to be at or near one value or the other, but spends little time between the two general values. The $V_{L,e}$ component indicates that at the position for run 51, the flow is at the lower velocity value most of the time; however at the position for run 52, the flow is at the higher velocity value most of the time. The positions are only 0.007 chord lengths different in height (2.1 mm). These points are probably on opposite sides of the proposed shear layer. The most likely explanation of the double peak is that the shear layer is oscillatory. If the shear layer was steady, the double peaks would probably not exist, and a shift in velocity would occur as the measurement location was traversed through it. This was believed to be an oscillating shear layer from a laminar-separation bubble. The laminar separation bubble was justified by a similar situation reported in reference 20. An NACA 0010 (modified) airfoil was tested to determine its characteristics when laminar separation was developed. Reference 20 indicates that at a Reynolds number of 1.5×10^6 at 4.75° angle of attack, the NACA 0010 (modified) airfoil should have a laminar separation at approximately $x_c/c = 0.02$, and the flow should make the transition from laminar to turbulent and reattach at $x_c/c = 0.05$. Realizing that the present investigation of the NACA 0012 airfoil was at a Reynolds number of 1×10^6 at $\alpha = 4.75^\circ$, it seems entirely possible that the phenomenon observed was a laminar-separation bubble. The oscillation of the shear layer was justified by the skewed histograms ahead of this point on the airfoil. A skewed histogram, as explained in appendix B of reference 2, indicates a fluctuation primarily in flow angle. Thus, the flow was experiencing variations in velocity and angle. The position of the laminar-separation point as measured in reference 20 was found to be highly sensitive to slight wing angle-of-attack changes; therefore, it is possible that the separation point was moving with the flow-angle oscillation. This unsteadiness in separation point would result in unsteadiness in the shear layer of the separation and trigger an undulating shear layer.

References 21 and 22 provide an analysis of the effects of the separation bubble on airfoils. Reference 21 in particular indicates that local surface velocities just ahead of the bubble are lower than those without the bubble. The local surface velocities downstream are increased by the presence of the bubble, and if the bubble reattaches, the velocities approach those of the airfoil without the bubble. The data presented in reference 2 are summarized in figure 48 and indicate similar trends; that is, ahead of the airfoil and the proposed laminar-separation bubble, the theoretically computed velocities (without laminar-separation bubble) are higher than the experimentally measured velocities (with laminar-separation bubble). Figure 48 indicates that downstream of $x_c/c = 0.7$ the experimental values are larger than the theoretical values, and at the trailing edge the velocities compare favorably. This would indicate, based on the analysis in reference 22, that the bubble began near the leading edge and reattached downstream.

CONCLUDING REMARKS

An analytical investigation was conducted using two methods to determine the flow field at the center line of an unswept wing with an aspect ratio of eight. The analysis used a two-dimensional viscous-flow prediction technique for the flow-field calculation and a three-dimensional potential-flow panel method to evaluate the degree of two-dimensionality achieved at the wing center line.

The three-dimensional potential-flow program results differed very little from the two-dimensional viscous-flow program results (outside the boundary layer), which indicates essentially two-dimensional flow conditions at the measurement location.

The agreement between experiment and these theories indicated that both the theoretical techniques and the experiment provided true representations of the velocity field about the airfoil.

Measurements within the very small wake region of this airfoil were obtained and indicated a typical velocity defect.

The data for the wing at $\alpha = 4.75^\circ$ indicated that a laminar-separation bubble probably existed with a thin oscillating shear layer. The prediction technique did not model this bubble; therefore, in the area of the bubble, the correlation was poor.

Langley Research Center
National Aeronautics and Space Administration
Hampton, VA 23665 March 15, 1978

REFERENCES

1. Young, Warren H., Jr.; Meyers, James F.; and Hepner, Timothy E.: *Laser Velocimeter Systems Analysis Applied to a Flow Survey Above a Stalled Wing*. NASA TN D-8408, 1977.

2. Hoad, Danny R.; Meyers, James F.; Young, Warren H., Jr.; and Hepner, Timothy E.: *Laser Velocimeter Survey About a NACA 0012 Wing at Low Angles of Attack*. NASA TM-74040, 1978.

3. Meyers, James F.; Feller, William V.; and Hepner, Timothy E.: *A Feasibility Test of the Laser Velocimeter in the Mach 5 Nozzle Test Chamber*. Proceedings of the Second International Workshop on Laser Velocimetry, Volume I, H. D. Thompson and W. H. Stevenson, eds., Eng. Exp. Stn. Bull. No. 144, Purdue Univ., 1974, pp. 290-313.

4. Whiff en, M. C.; and Meadows, D. M.: *Two Axis, Single Particle Laser Velocimeter System for Turbulence Spectral Analysis*. Proceedings of the Second International Workshop on Laser Velocimetry, Volume I, H. D. Thompson and W. H. Stevenson, eds., Eng. Exp. Stn. Bull. No. 144, Purdue Univ., 1974, pp. 1-15.

5. Eggins, P. L.; and Jackson, D. A.: *Laser-Doppler Velocity Measurements in an Under-Expanded Free Jet*. J. Phys. D: Appl. Phys., vol. 7, no. 14, Sept. 21, 1974, pp. 1894-1906.

6. Goldman, Louis J.; Seasholtz, Richard G.; and McLallin, Kerry L.: *Velocity Surveys in a Turbine Stator Annular-Cascade Facility Using Laser Doppler Techniques*. NASA TN D-8269, 1976.

7. Wilson, John C.: *A General Rotor Model System for Wind-Tunnel Investigations*. J. Aircr., vol. 14, no. 7, July 1977, pp. 639-643.

8. Sullivan, John P.: *An Experimental Investigation of Vortex Rings and Helicopter Rotor Wakes Using a Laser Doppler Velocimeter*. Tech. Rep. No. 183 (Contract No. N00019-72-C-0450), Massachusetts Inst. Technol., June 1973. (Available from DDC as AD 778 768.)

9. Johnson, Bruce V.: *LDV Measurements in the Periodic Velocity Field Adjacent to a Model Helicopter Rotor*. Proceedings of the Second International Workshop on Laser Velocimetry, Volume II, H. D. Thompson and W. H. Stevenson, eds., Eng. Exp. Stn. Bull. No. 144, Purdue Univ., 1974, pp. 169-181.

10. Landgrebe, Anton J.; and Johnson, Bruce V.: *Measurement of Model Helicopter Rotor Flow Velocities With a Laser Doppler Velocimeter*. J. American Helicopter Soc., vol. 19, no. 3, July 1974, pp. 39-43.

11. Biggers, James C.; and Orloff, Kenneth L.: *Laser Velocimeter Measurements of the Helicopter Rotor-Induced Flow Field*. J. American Helicopter Soc., vol. 20, no. 1, Jan. 1975, pp. 2-10.

12. Hsieh, Tsuying: *Analysis of Velocity Measurements About a Hemisphere-Cylinder Using a Laser Velocimeter*. J. Spacecr. & Rockets, vol. 14, no.,5, May 1977, pp. 280-283.

13. Meyers, James F.; Couch, Lana M; Feller, William V.; and Walsh, Michael J.: *Laser Velocimeter Measurements in a Large Transonic Wind Tunnel*. Minnesota Symposium on Laser Anemometry - Proceedings, E. R. G. Eckert, ed., Univ. of Minnesota, Oct. 1975, pp. 84-111.

14. Smetana, Frederick O.; Summey, Delbert C.; Smith, Neill S.; and Carden, Ronald K.: *Light Aircraft Lift, Drag, and Moment Prediction - A Review and Analysis*. NASA CR-2523, 1975.

15. McGhee, Robert J.; and Beasley, William D.: *Low-Speed Aerodynamic Characteristics of a 17-Percent-Thick Airfoil Section Designed for General Aviation Applications*. NASA TN D-7428, 1973.

16. Hess, John L.: *Calculation of Potential Flow About Arbitrary Three-Dimensional Lifting Bodies*. Rep. No. MDC J5679-01 (Contract N00019-71-C-0524), McDonnell Douglas Corp., Oct. 1972. (Available from DDC as AD 755 480.)

17. Mechtly, E. A.: *The International System of Units - Physical Constants and Conversion Factors* (Second Revision) . NASA SP-7012, 1973.

18. Yule, G. Udny; and Kendall, M. G.: **An Introduction to the Theory of Statistics**. Charles Griffin & Co., Ltd., 1940.

19. Meyers, James F.; and Walsh, Michael J.: *Computer Simulation of a Fringe Type Laser Velocimeter*. Proceedings of the Second International Workshop on Laser Velocimetry, Volume I, H. D. Thompson and W. H. Stevenson, eds., Eng. Exp. Stn. Bull. No. 144, Purdue Univ., 1974, pp. 471-510.

20. Gault, Donald E.: *An Experimental Investigation of Regions of Separated Laminar Flow*. NACA TN 3505, 1955.

21. Crabtree, L. F.: *Effects of Leading-Edge Separation on Thin Wings in Two-Dimensional Incompressible Flow*. J. Aeronaut. Sci., vol. 24, no. 8, Aug. 1957, pp. 597-604.

22. Ward, Julian W.: *The Behaviour and Effects of Laminar Separation Bubbles on Aerofoils in Incompressible Flow*. J. R. Aeronaut. Soc., vol 67, no. 636, Dec. 1963, pp. 783-790.

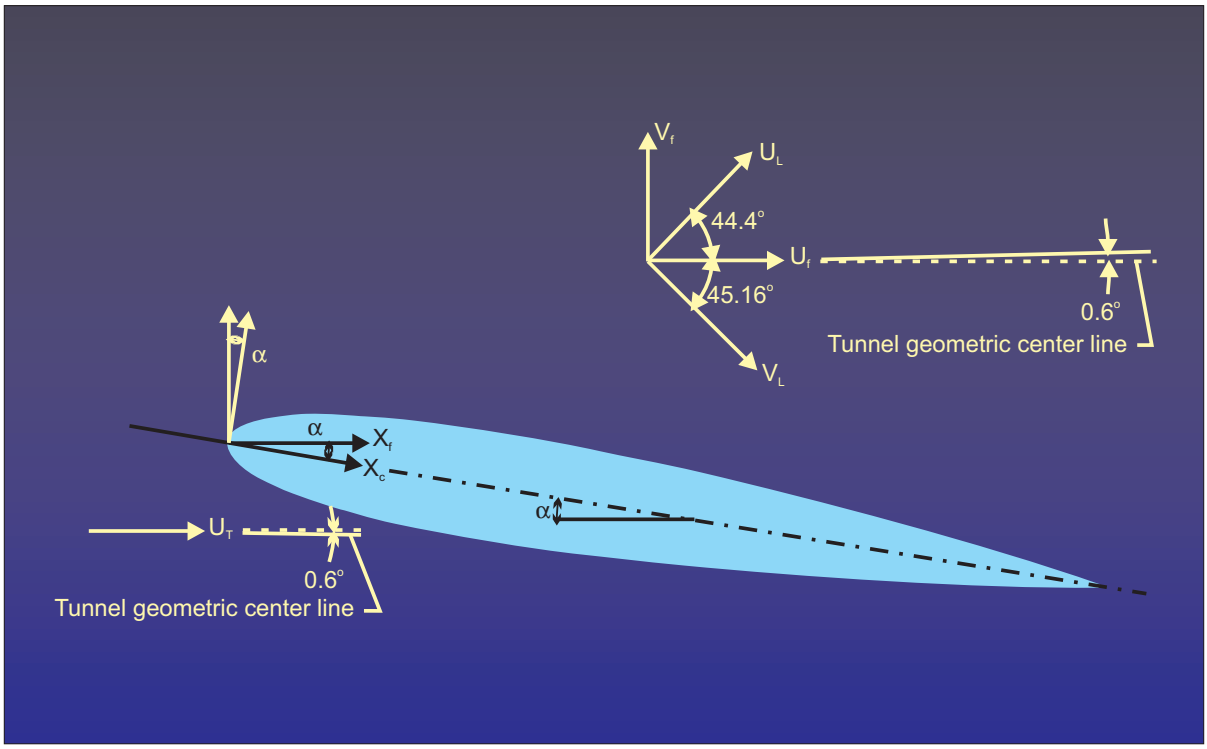

Figure 1.- Sketch of axis system used including directions of velocity components.

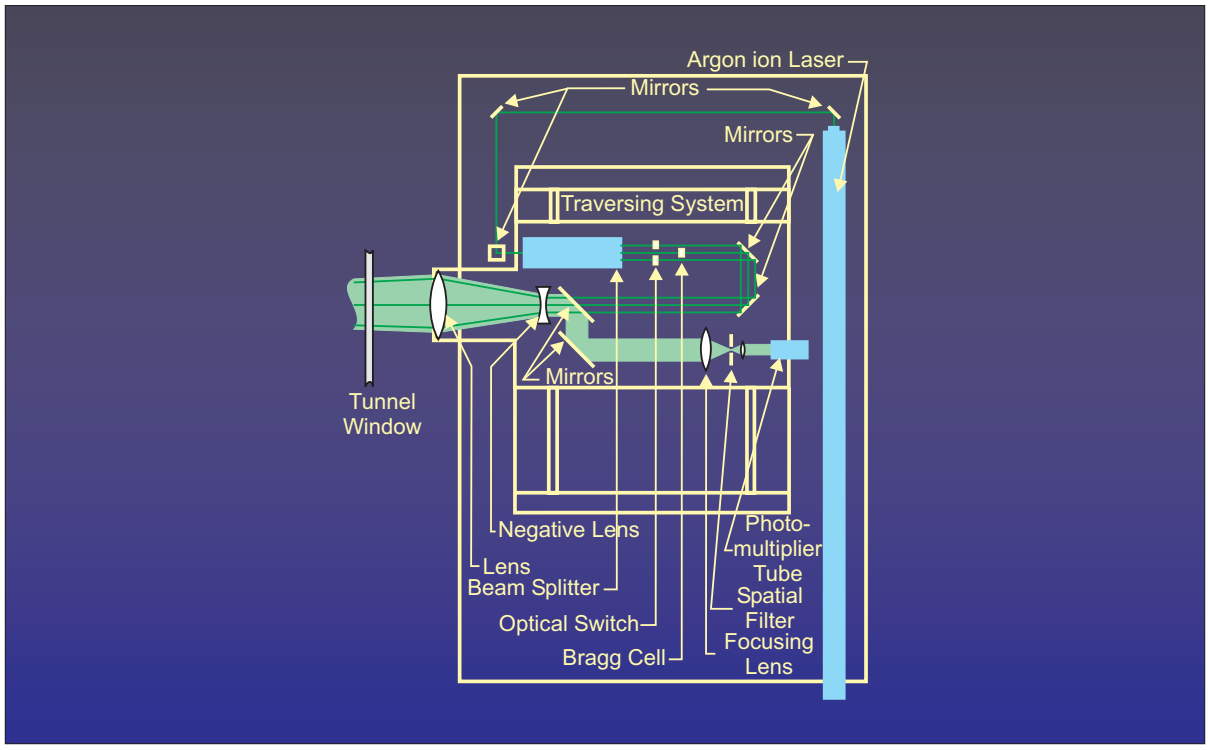

Figure 2.- Schematic of laser velocimeter optics.

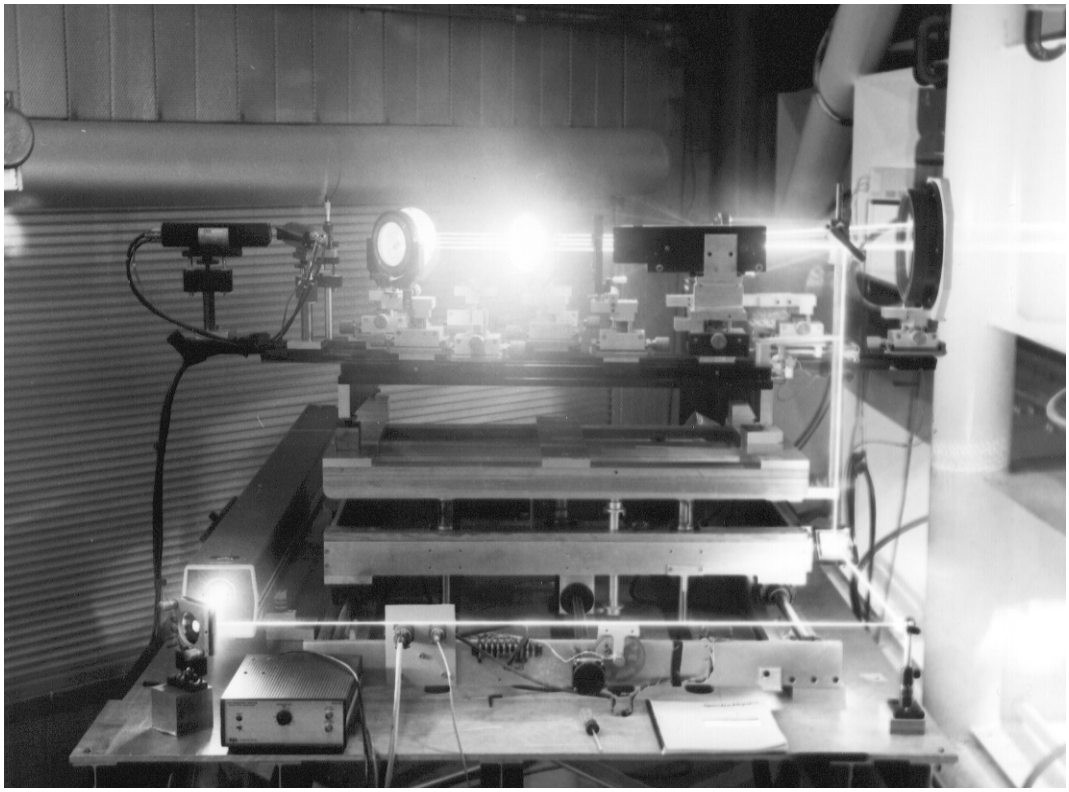

Figure 3.- Laser velocimeter optics platform in Langley V/STOL tunnel.

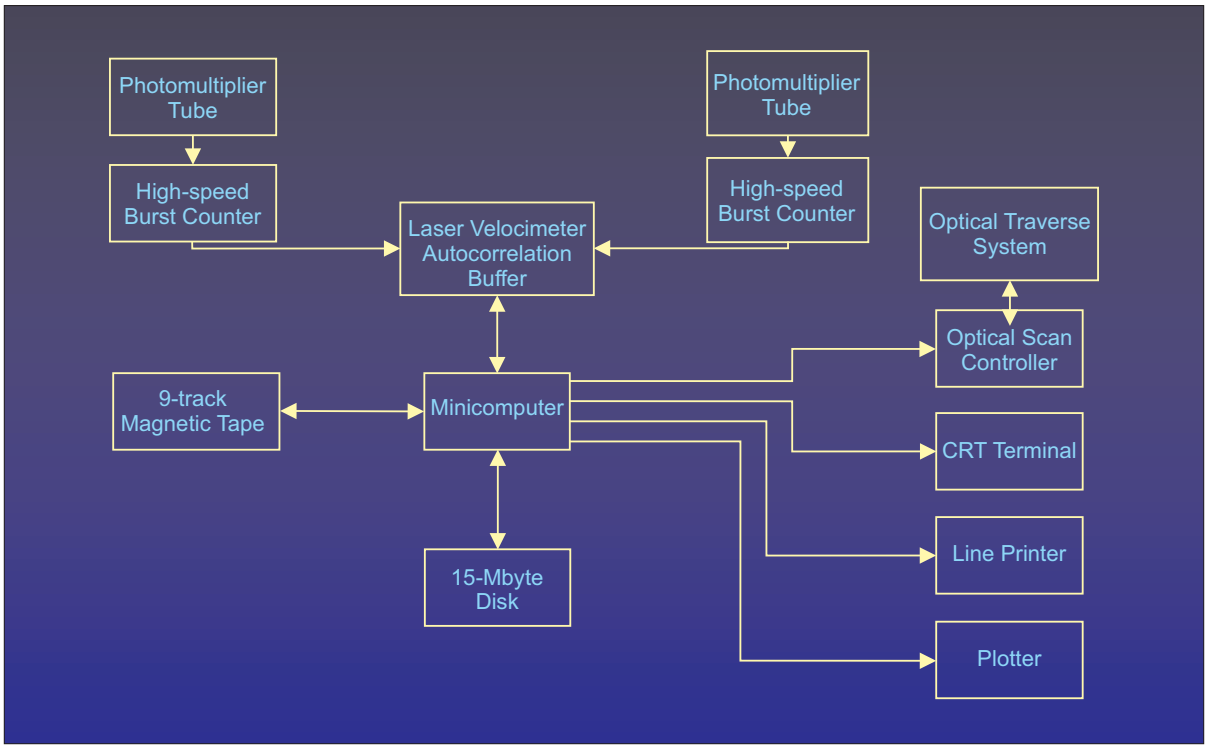

Figure 4.- Block diagram of laser velocimeter data-acquisition system.

Figure 5.- NACA 0012 wing installed in Langley V/STOL tunnel.

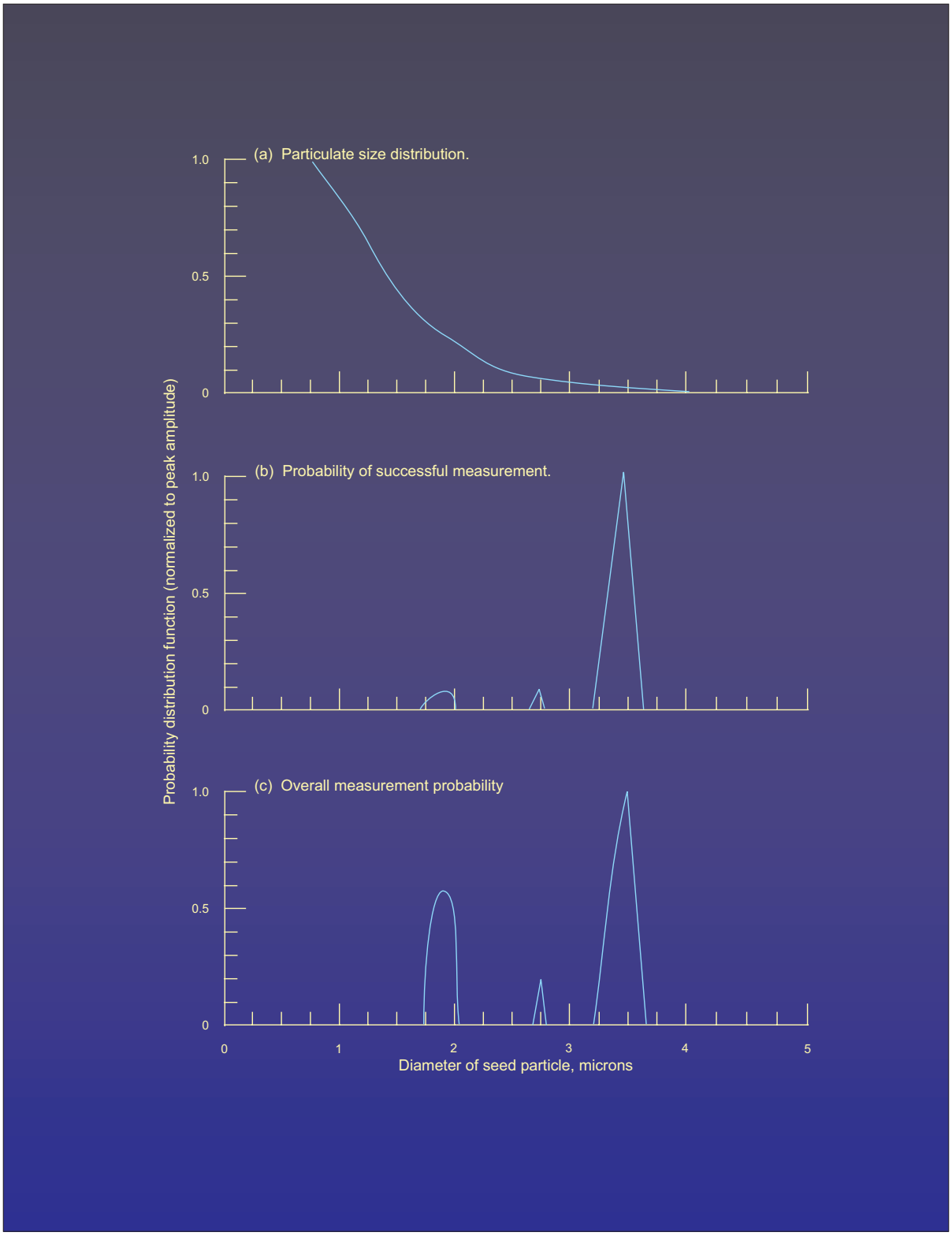

Figure 6.- Particle-size and probability distributions measured by laser velocimeter.

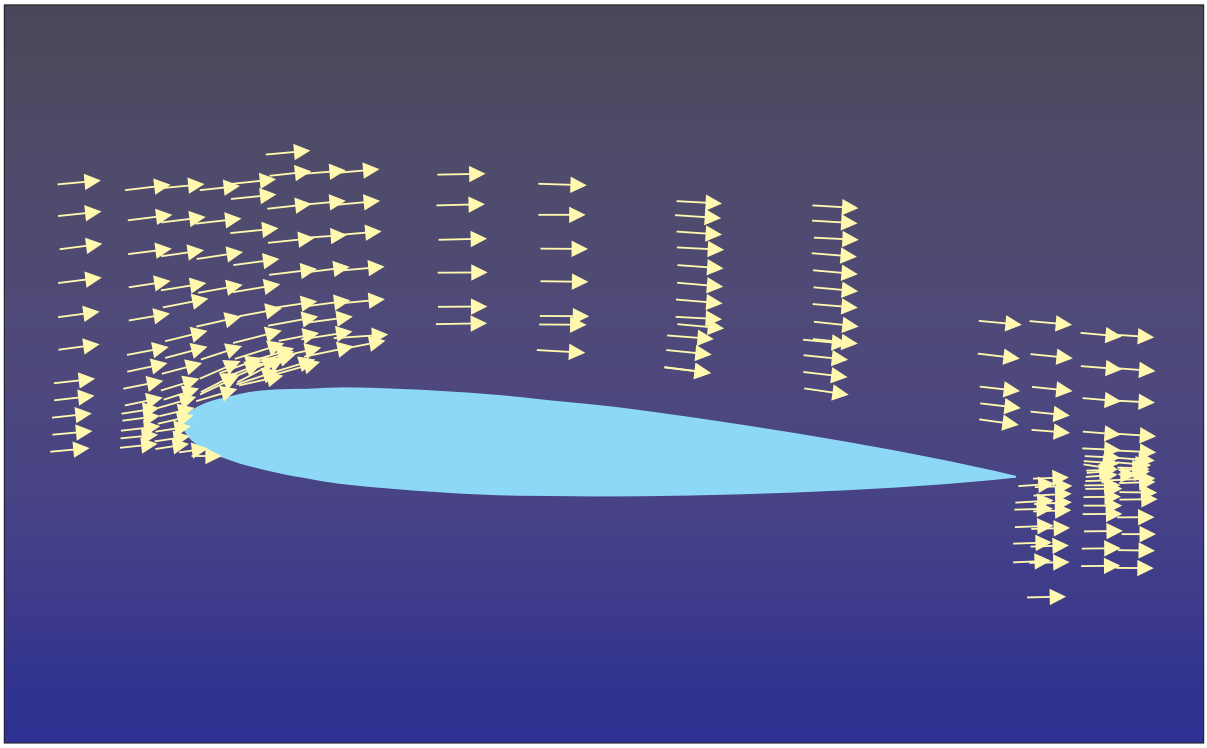

Figure 7.- Velocity vectors computed from measurements over wing at $\alpha = 4.75^{\circ}$.

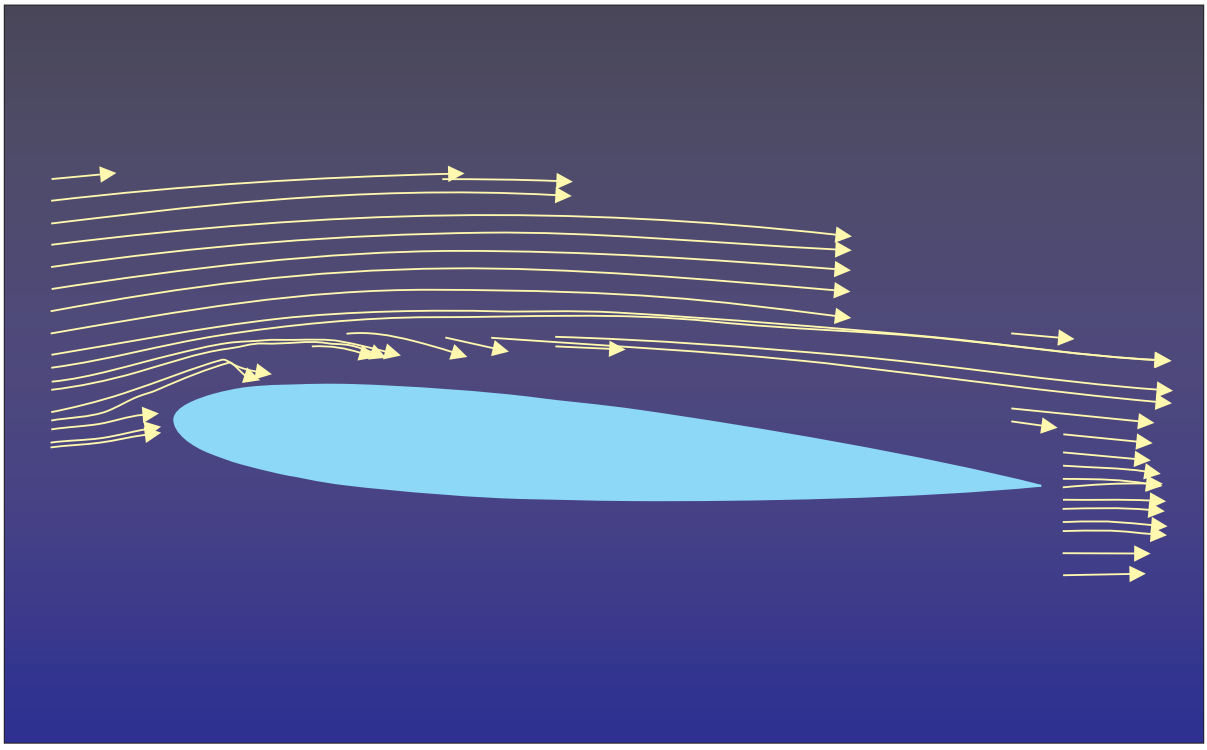

Figure 8.- Streamlines computed from interpolated flow-angle distribution over wing at $\alpha = 4.75^{\circ}$.

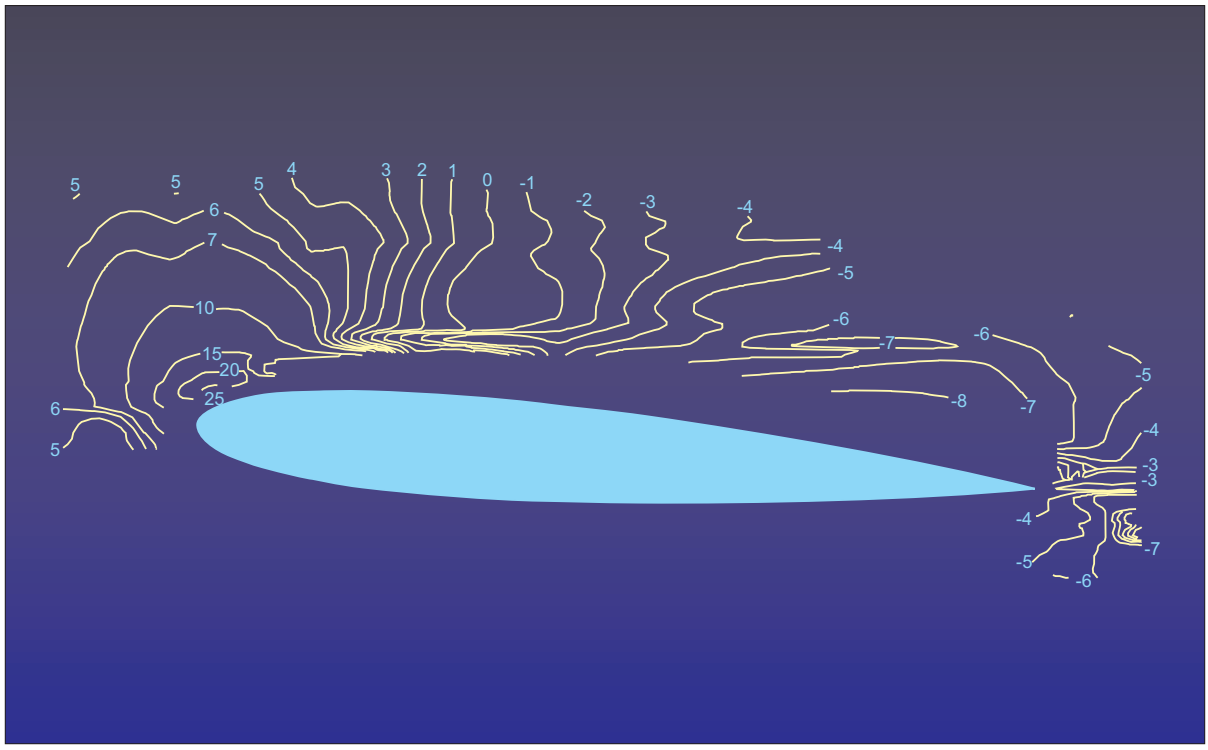

Figure 9.- Contours of constant local flow angle measured over wing at $\alpha = 4.75^{\circ}$.

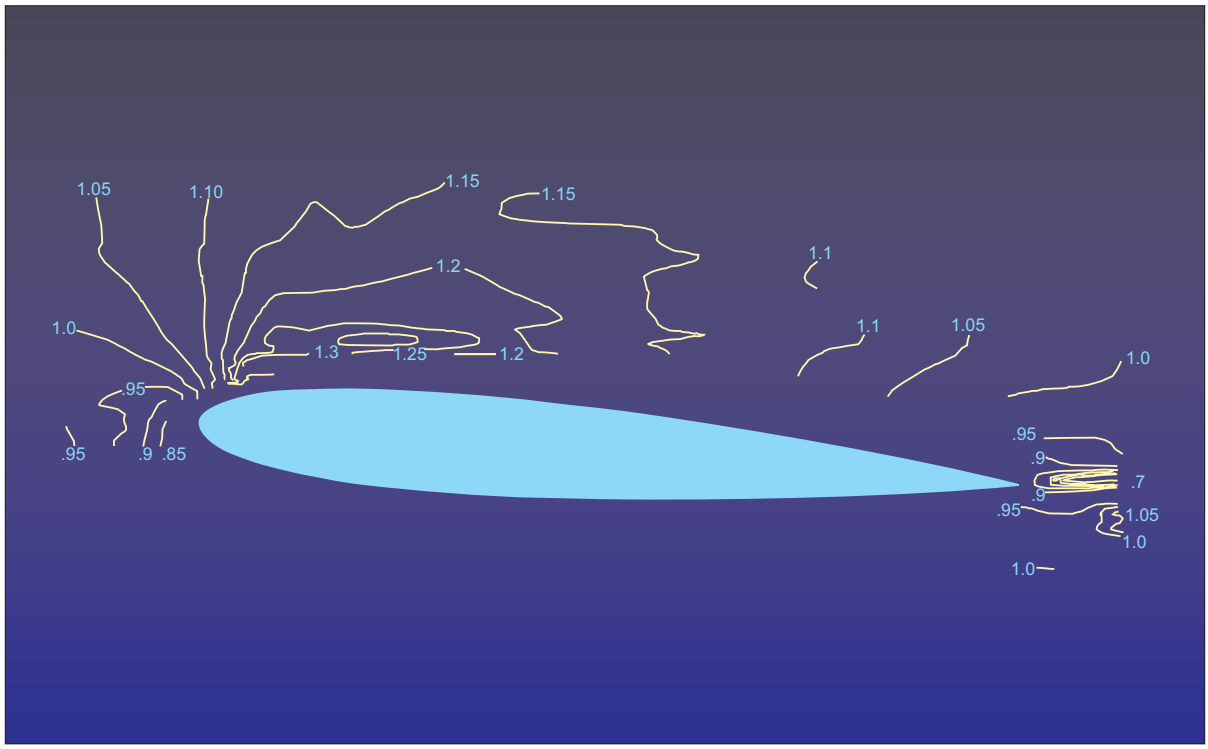

Figure 10.- Contours of constant $U_{R,e}/U_T$ measured over wing at $\alpha = 4.75^{\circ}$.

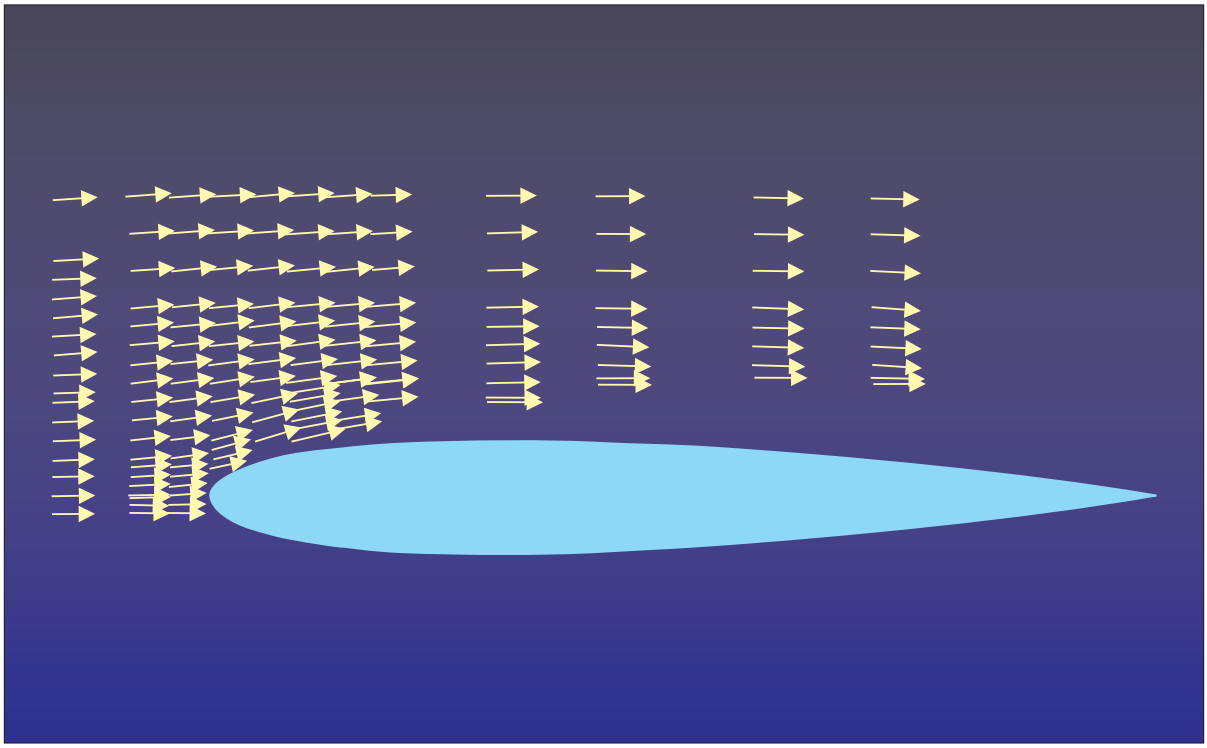

Figure 11.- Velocity vectors computed from measurements over wing at $\alpha = 0.6^{\circ}$.

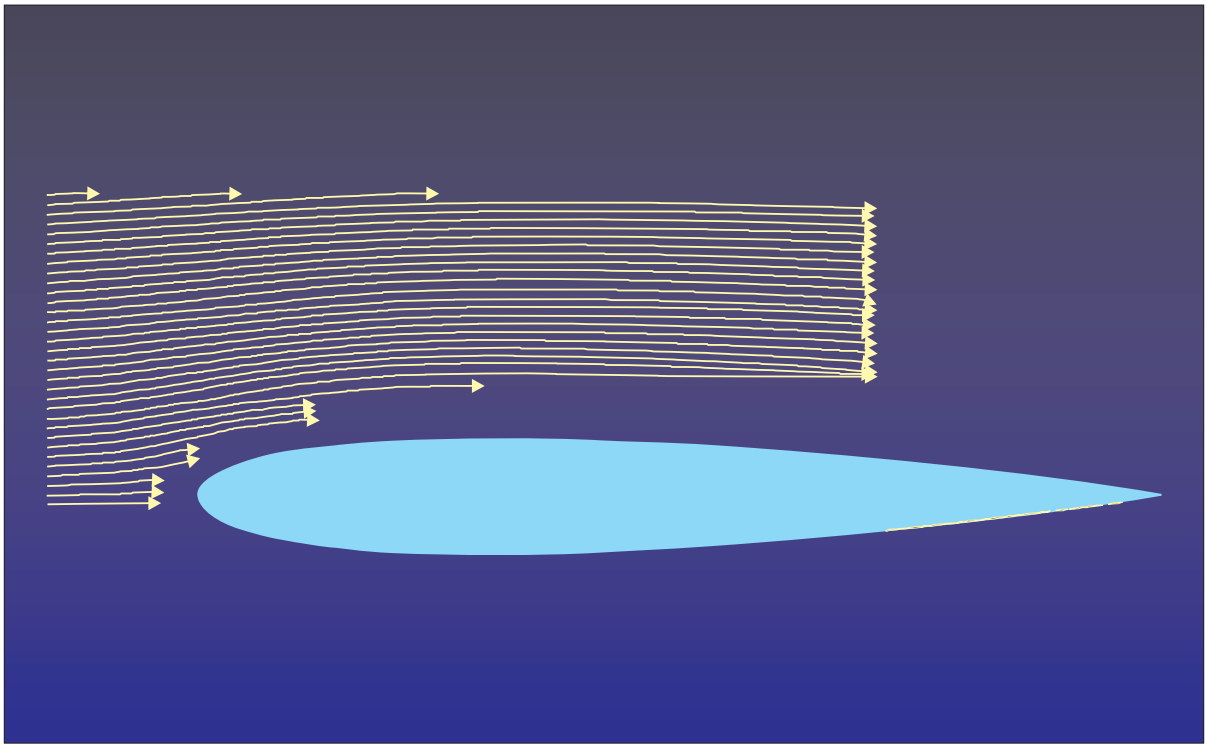

Figure 12.- Streamlines computed from interpolated flow-angle distribution over wing at $\alpha = 0.6^{\circ}$.

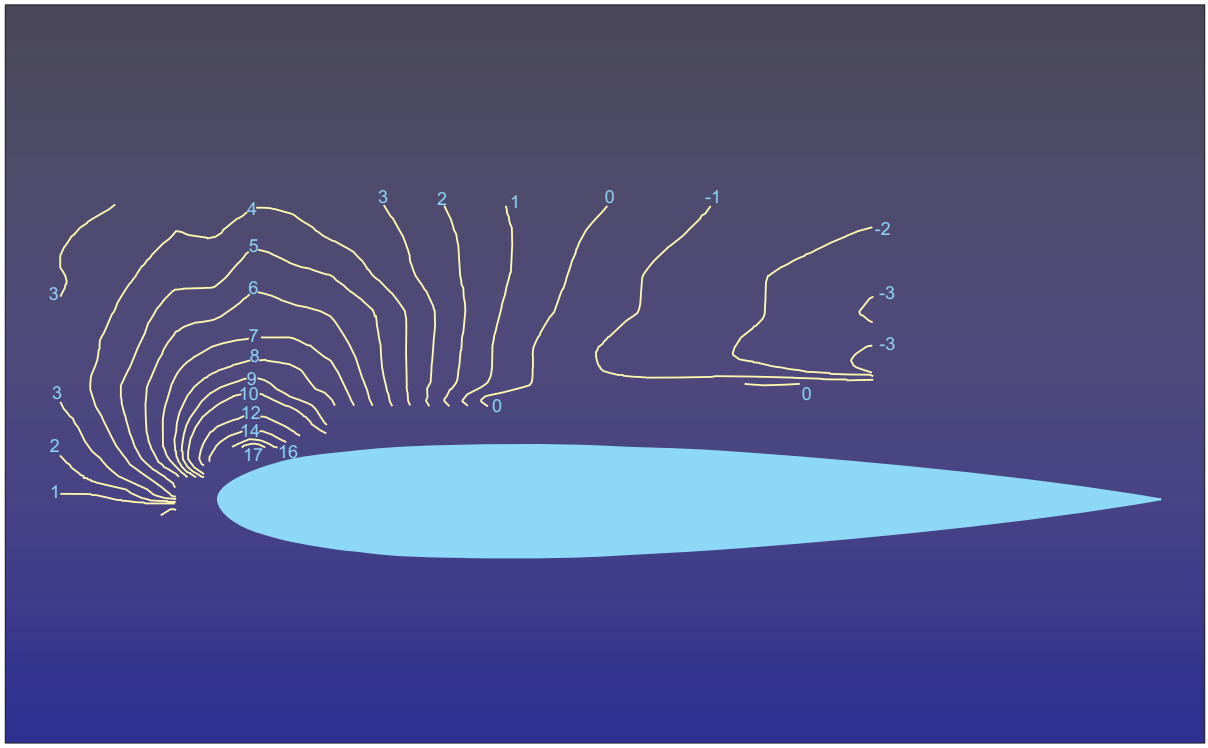

Figure 13.- Contours of constant local flow angle measured over wing at $\alpha = 0.6^{\circ}$.

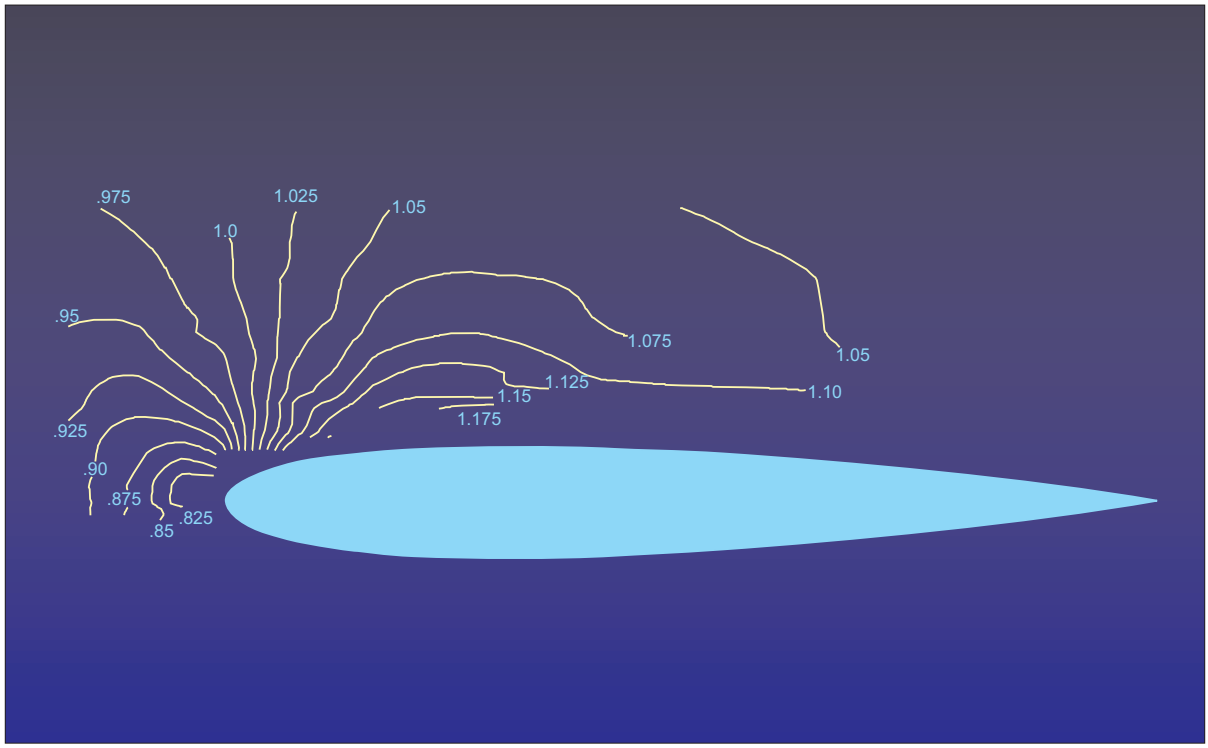

Figure 14.- Contours of constant $U_{R,e}/U_T$ measured over wing at $\alpha = 0.6^{\circ}$.

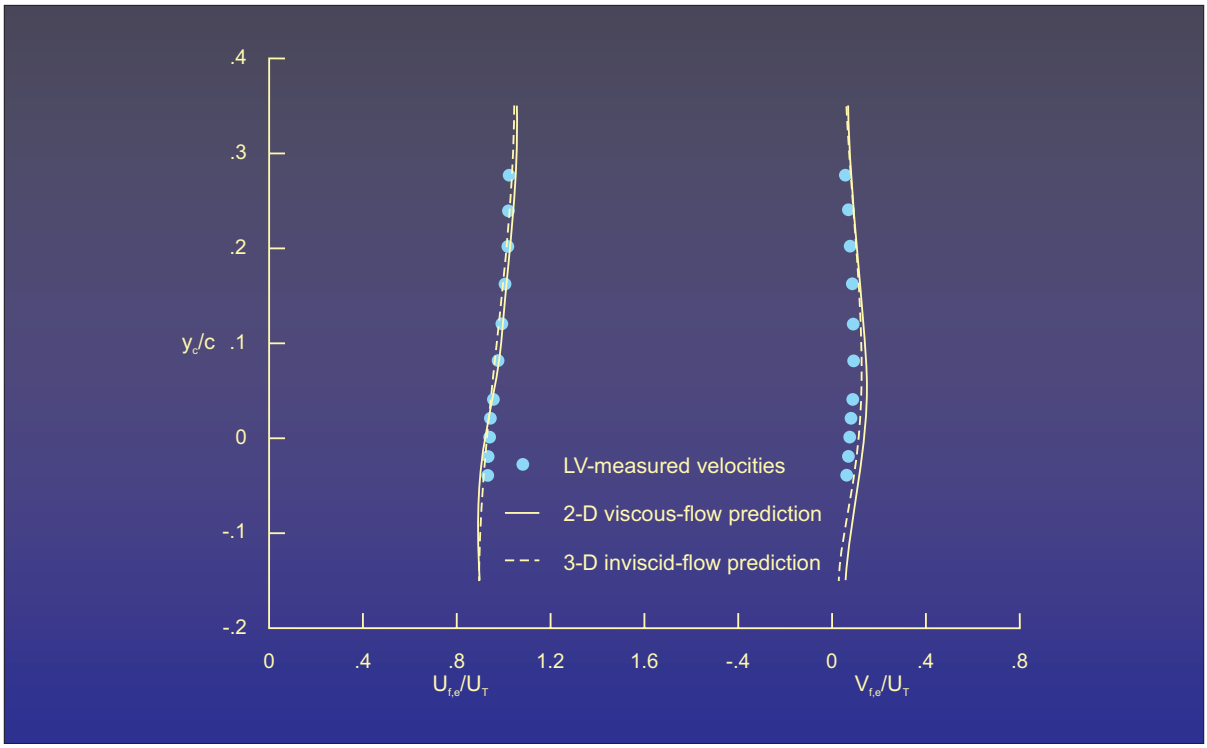

Figure 15.- Local velocity components along a scan perpendicular to wing chord at x_c/c = -0.16. $\alpha = 4.75^\circ$.

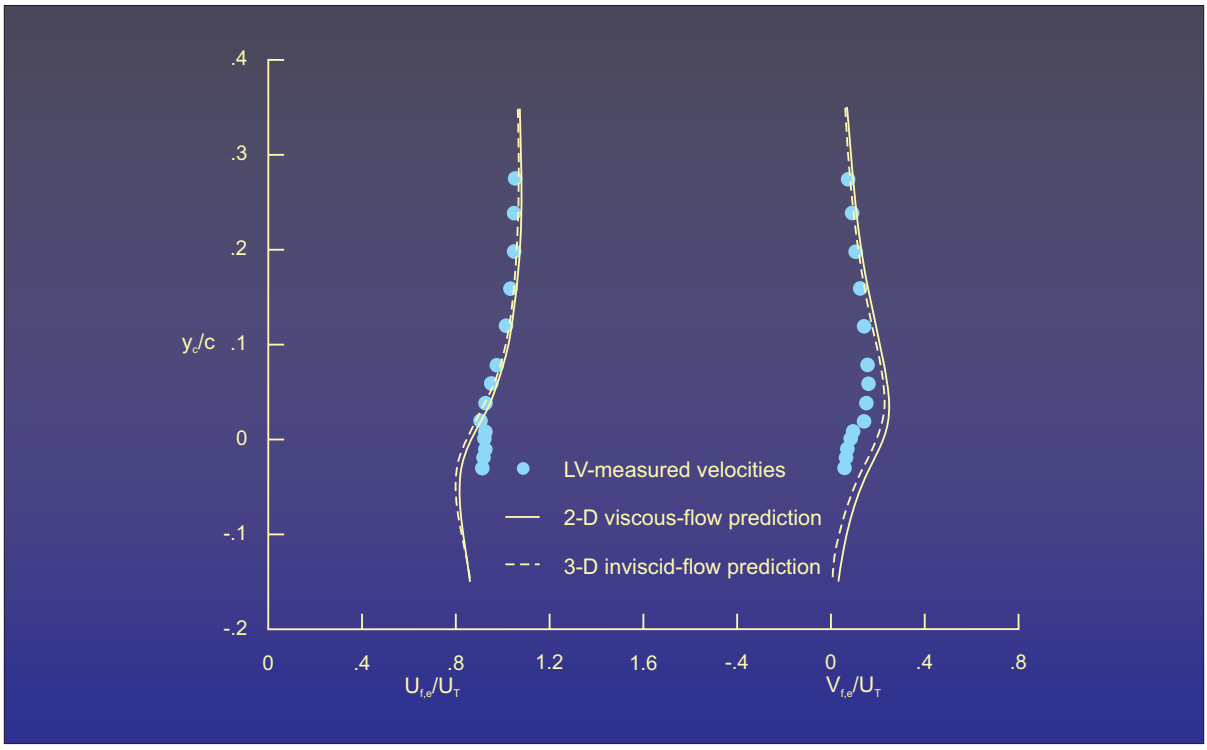

Figure 16.- Local velocity components along a scan perpendicular to wing chord at x_c/c = -0.08. $\alpha = 4.75^\circ$.

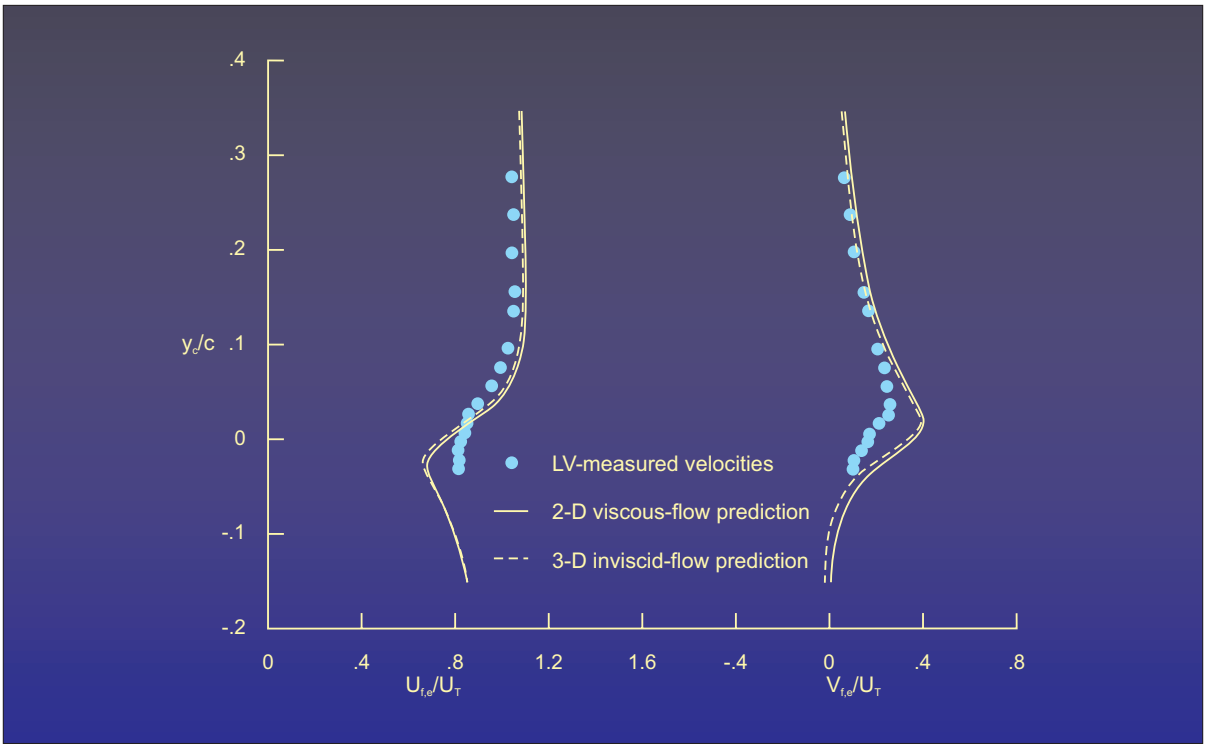

Figure 17.- Local velocity components along a scan perpendicular to wing chord at $x_c/c = -0.04$. $\alpha = 4.75^\circ$.

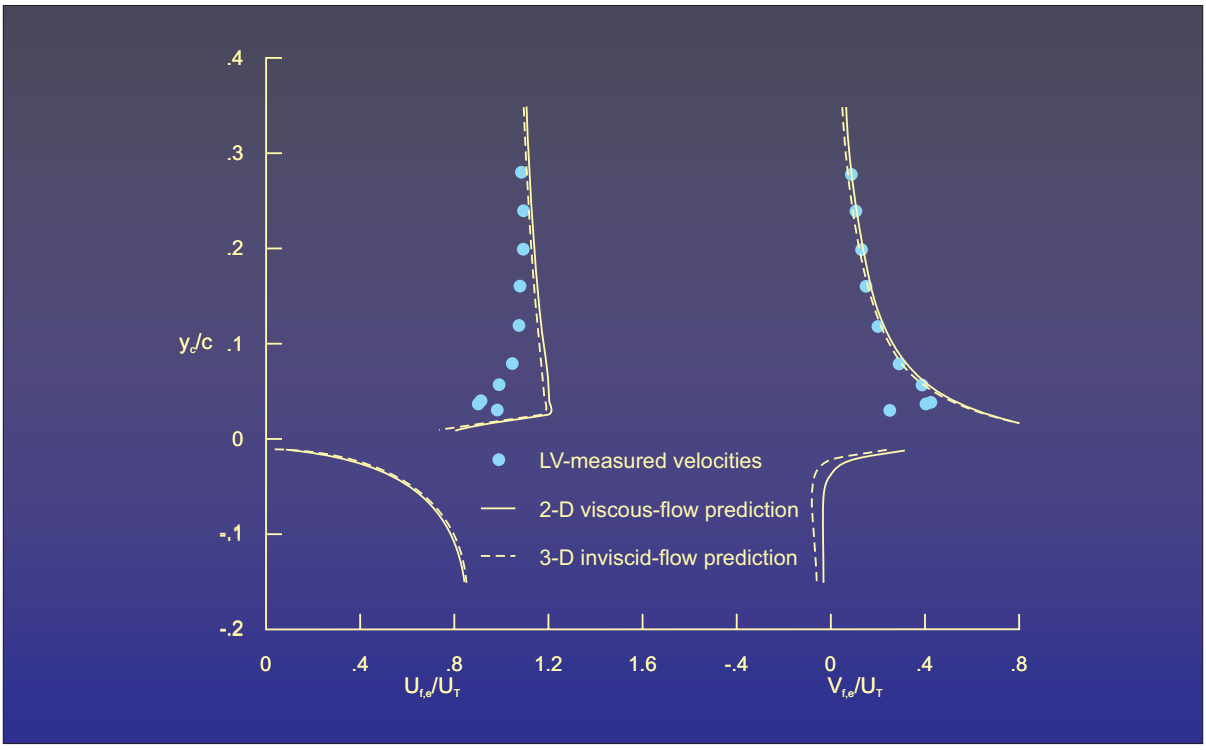

Figure 18.- Local velocity components along a scan perpendicular to wing chord at $x_c/c = 0$. $\alpha = 4.75^\circ$.

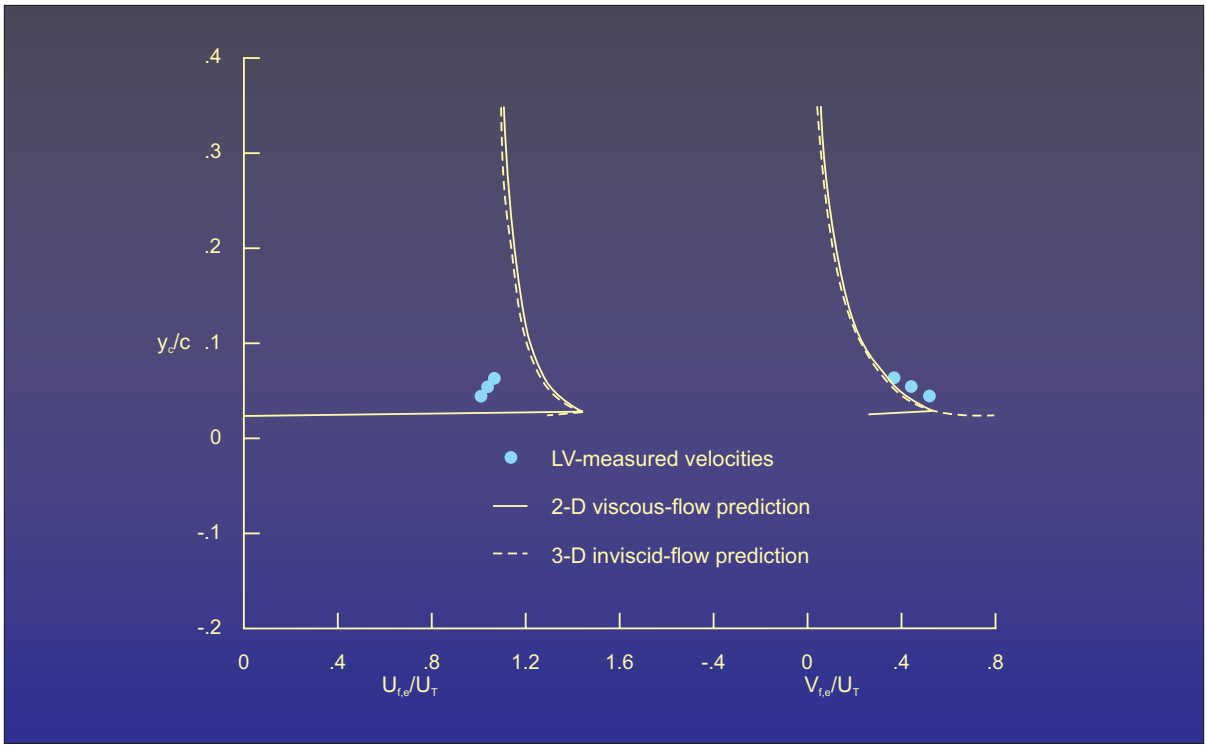

Figure 19.- Local velocity components along a scan perpendicular to wing chord at $x_c/c = 0.03$. $\alpha = 4.75°$.

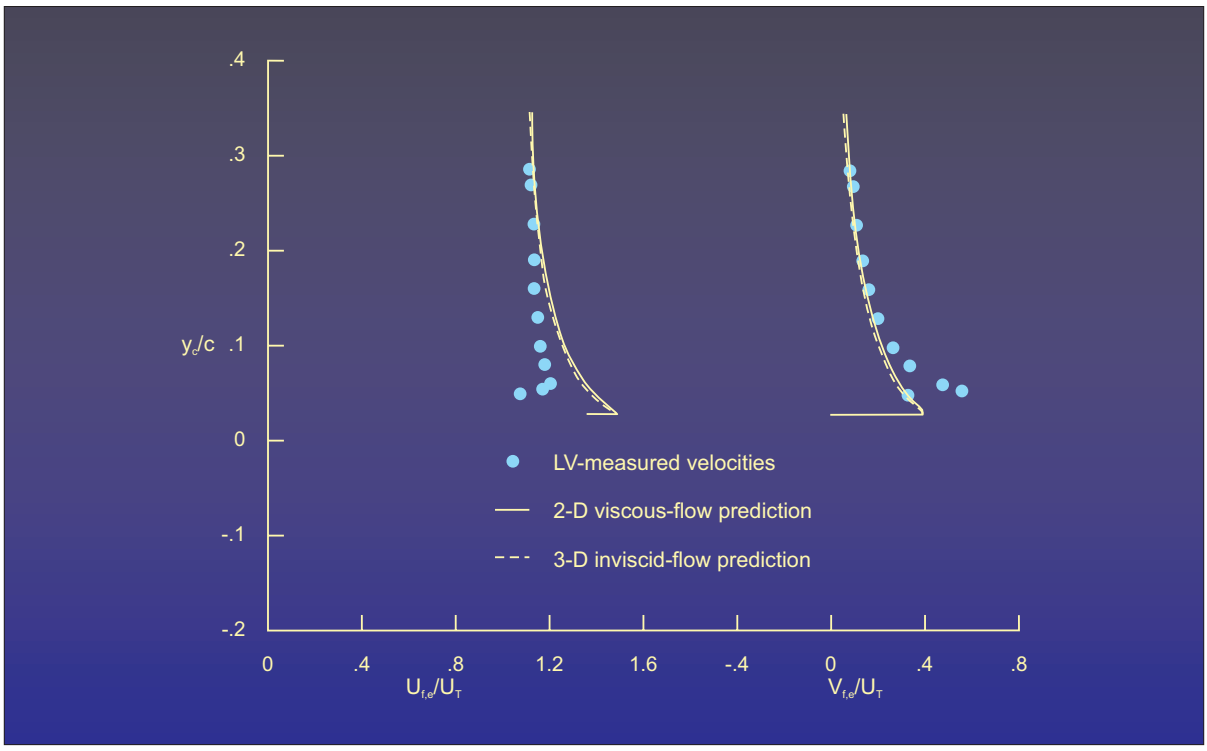

Figure 20.- Local velocity components along a scan perpendicular to wing chord at $x_c/c = 0.04$. $\alpha = 4.75°$.

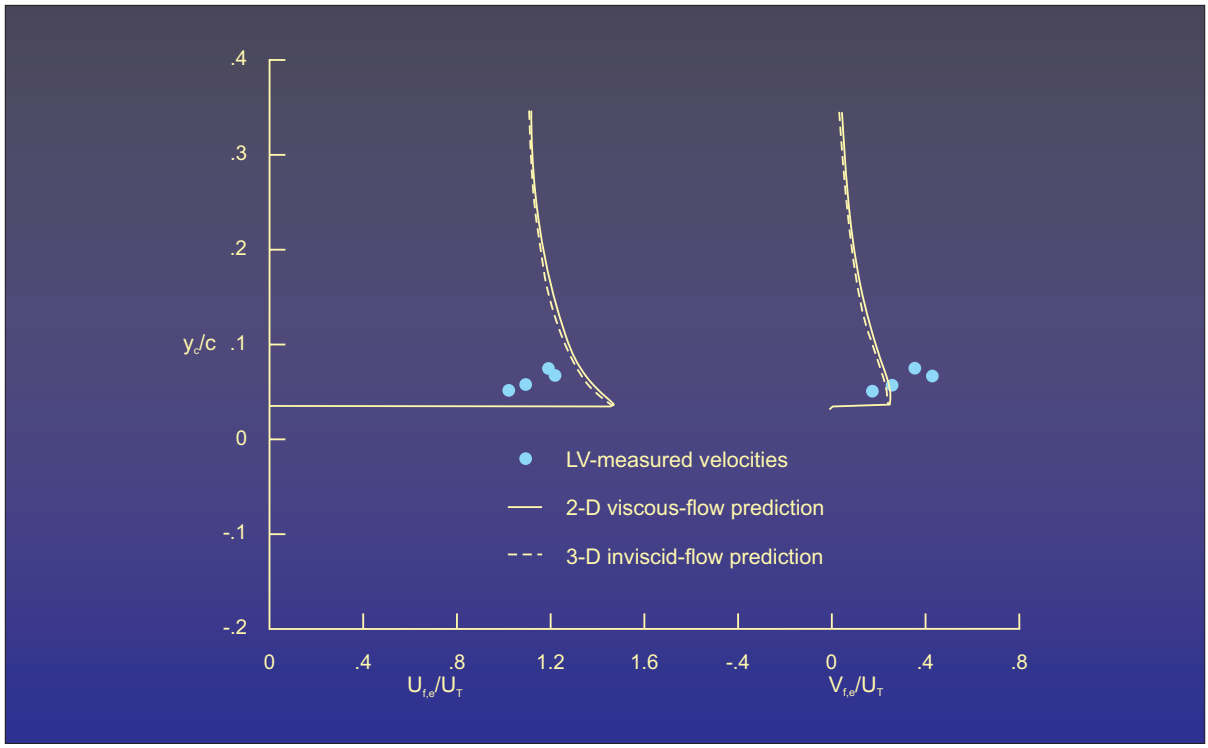

Figure 21.- Local velocity components along a scan perpendicular to wing chord at $x_c/c = 0.06$. $\alpha = 4.75°$.

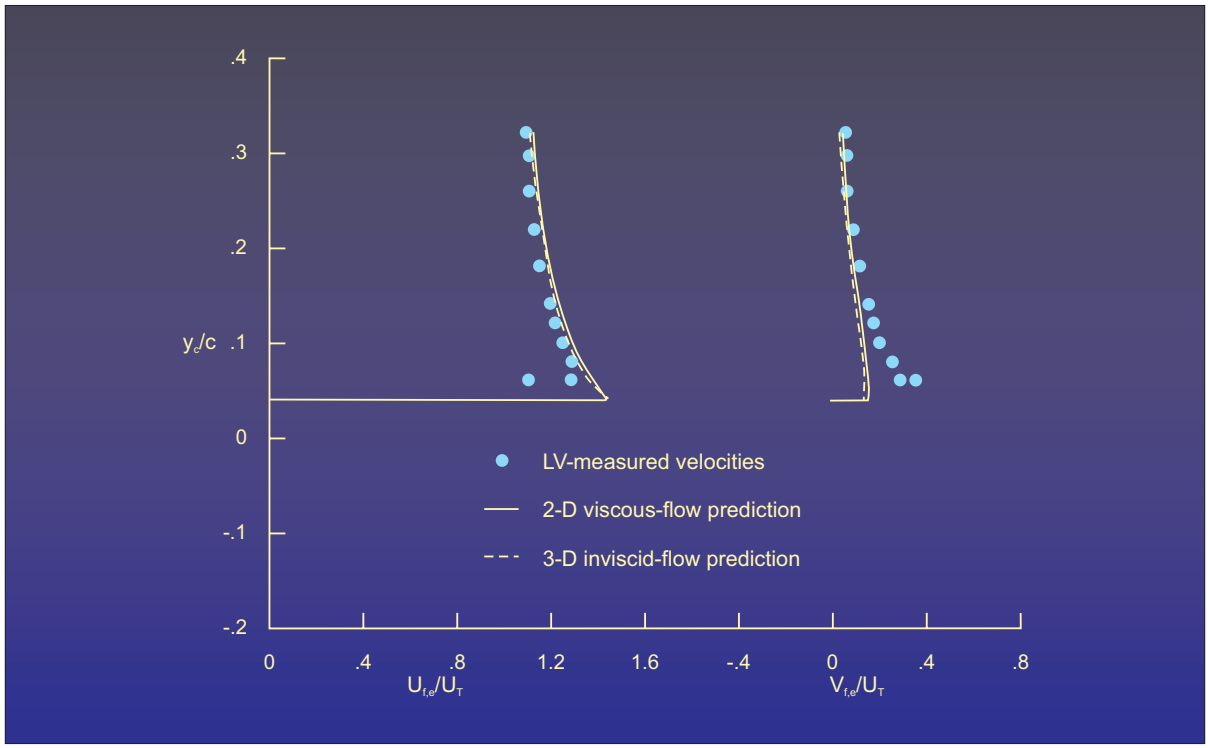

Figure 22.- Local velocity components along a scan perpendicular to wing chord at $x_c/c = 0.09$. $\alpha = 4.75°$.

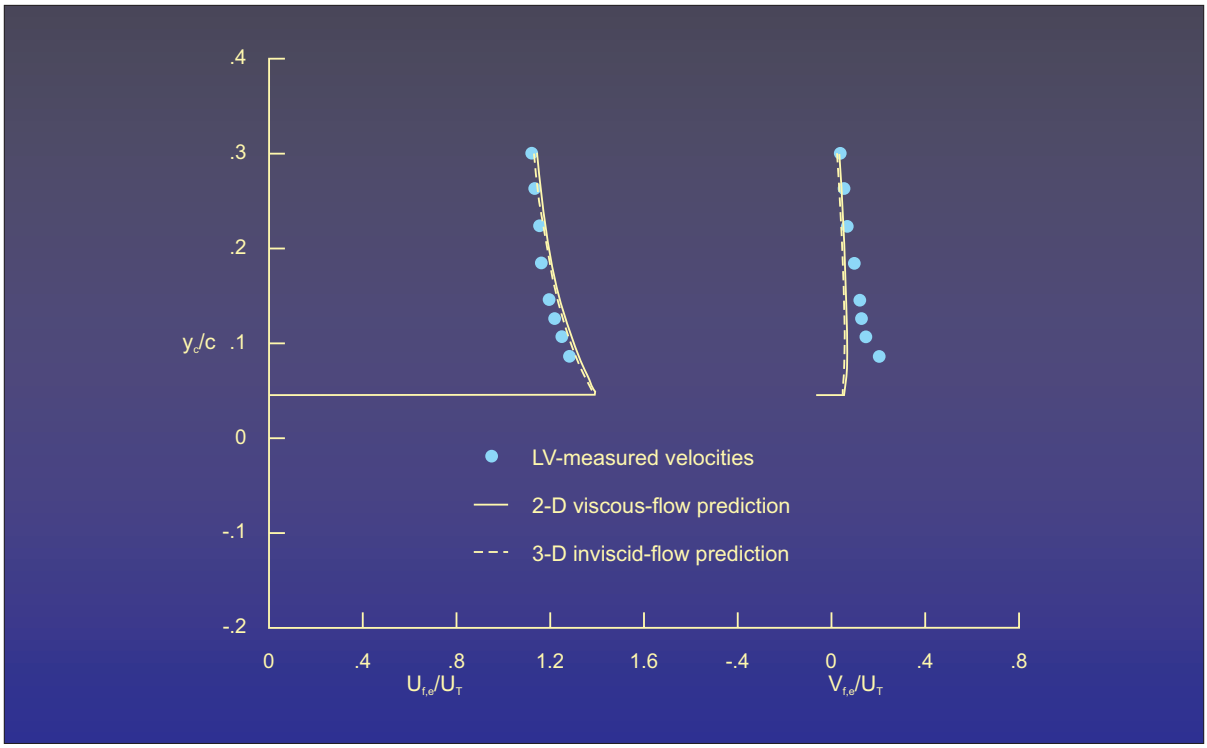

Figure 23.- Local velocity components along a scan perpendicular to wing chord at $x_c/c = 0.13$. $\alpha = 4.75^\circ$.

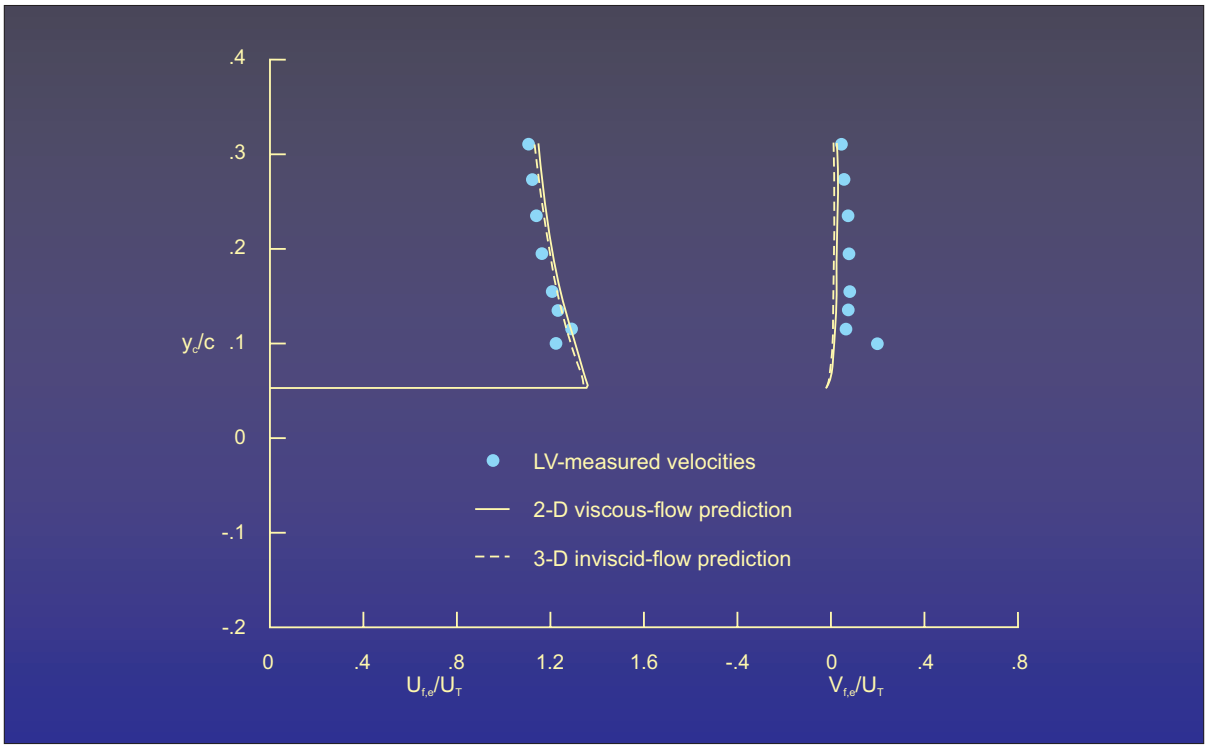

Figure 24.- Local velocity components along a scan perpendicular to wing chord at $x_c/c = 0.17$. $\alpha = 4.75^\circ$.

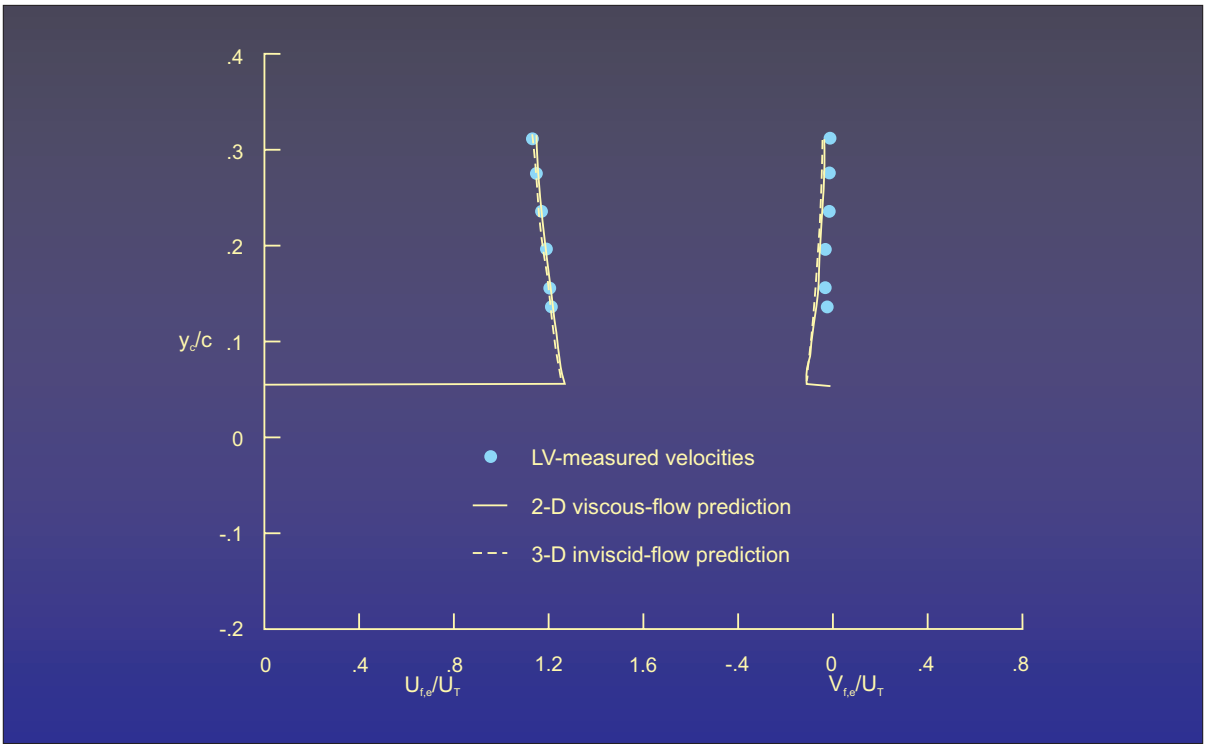

Figure 25.- Local velocity components along a scan perpendicular to wing chord at $x_c/c = 0.29$. $\alpha = 4.75°$.

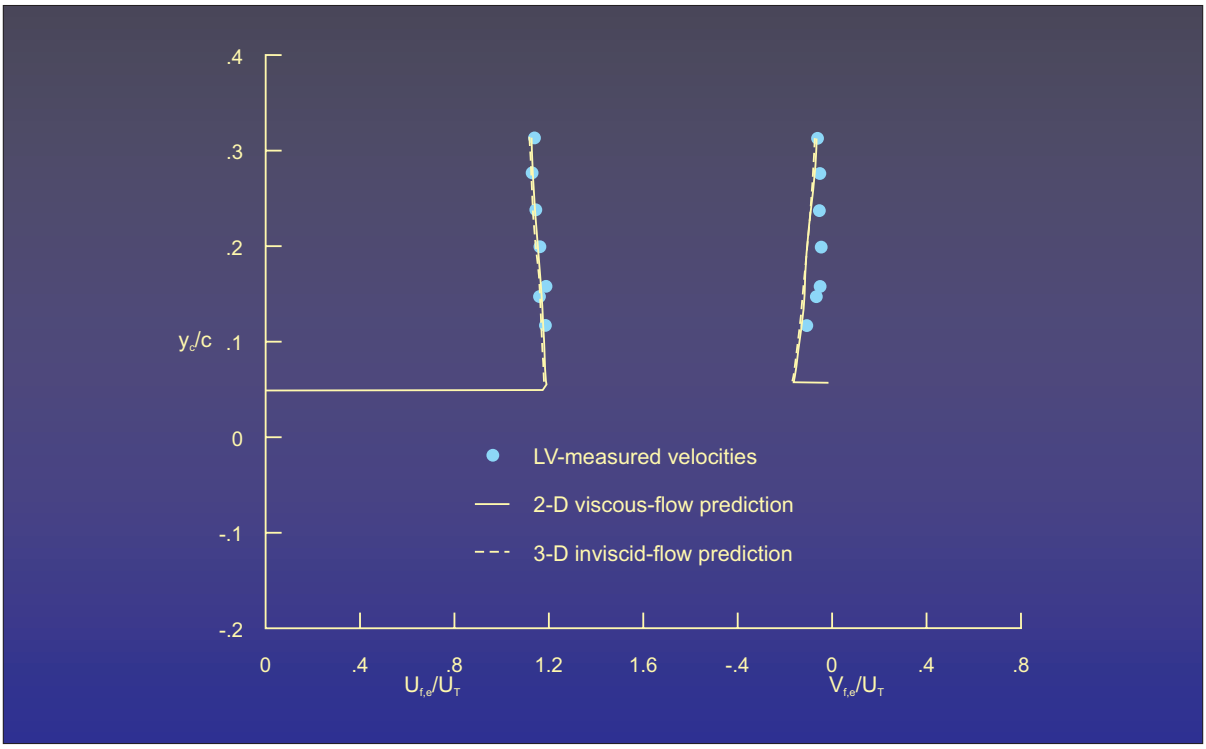

Figure 26.- Local velocity components along a scan perpendicular to wing chord at $x_c/c = 0.42$. $\alpha = 4.75°$.

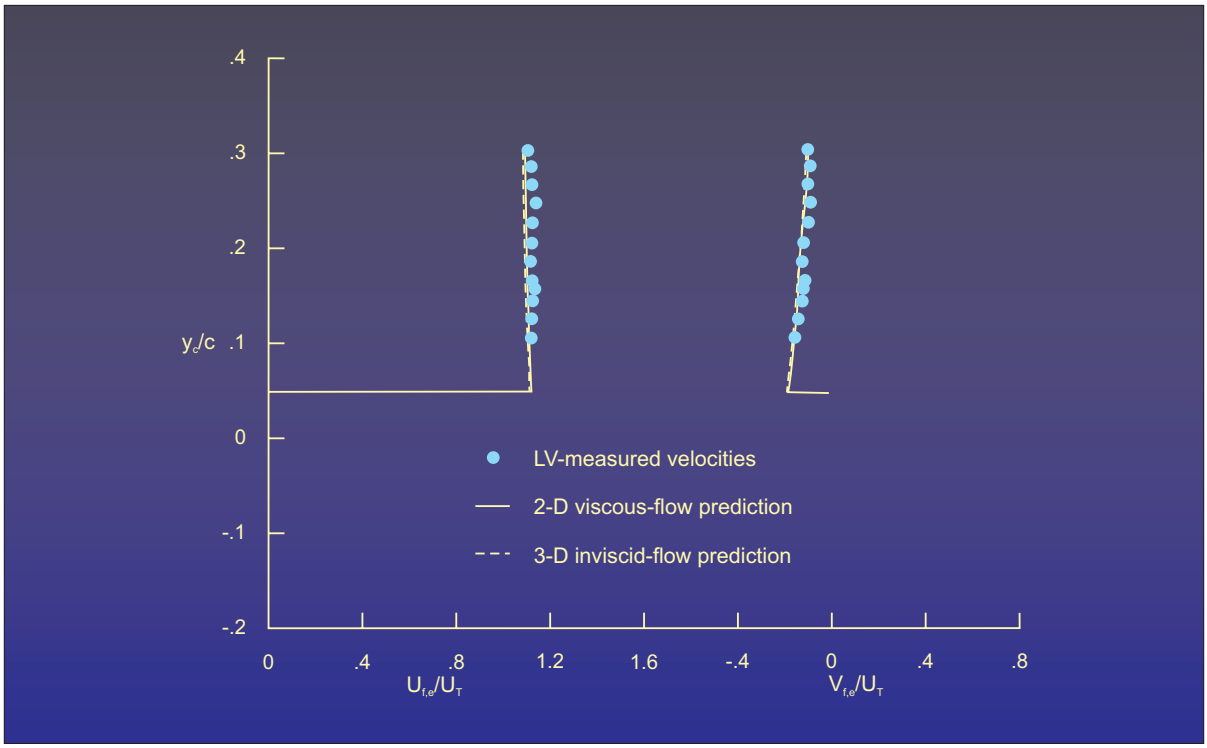

Figure 27.- Local velocity components along a scan perpendicular to wing chord at $x_c/c = 0.58$. $\alpha = 4.75°$.

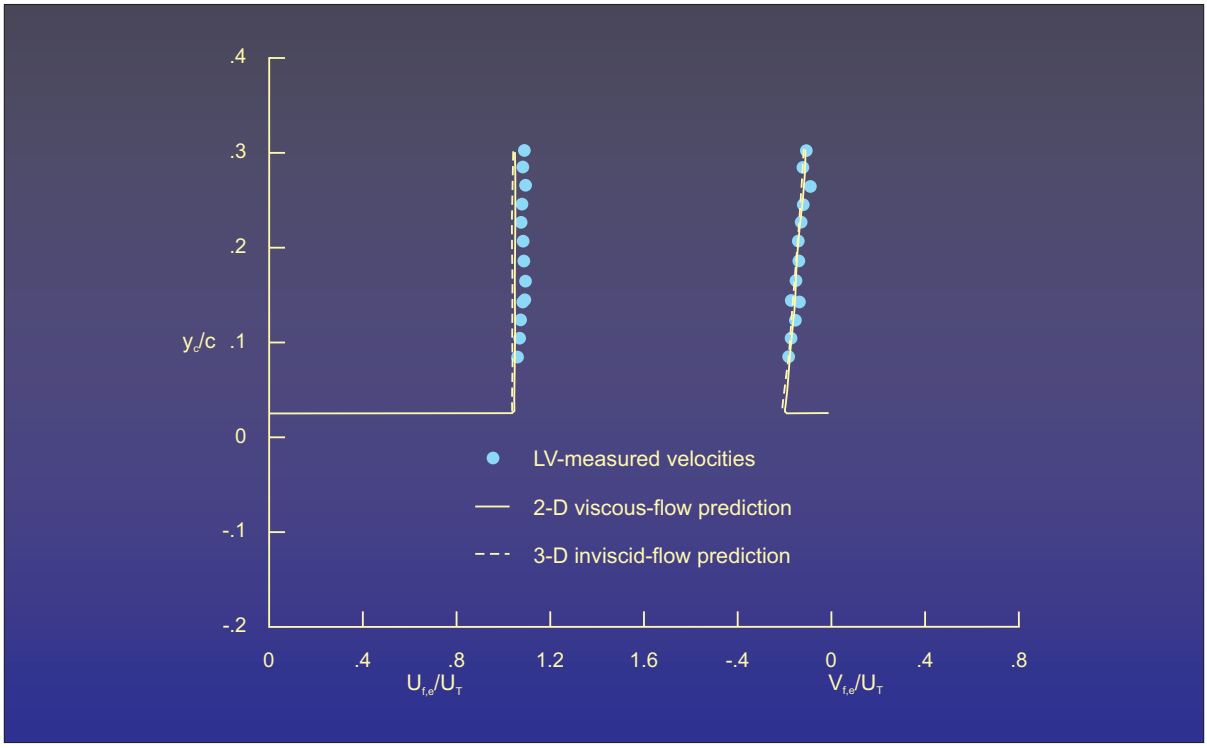

Figure 28.- Local velocity components along a scan perpendicular to wing chord at $x_c/c = 0.75$. $\alpha = 4.75°$.

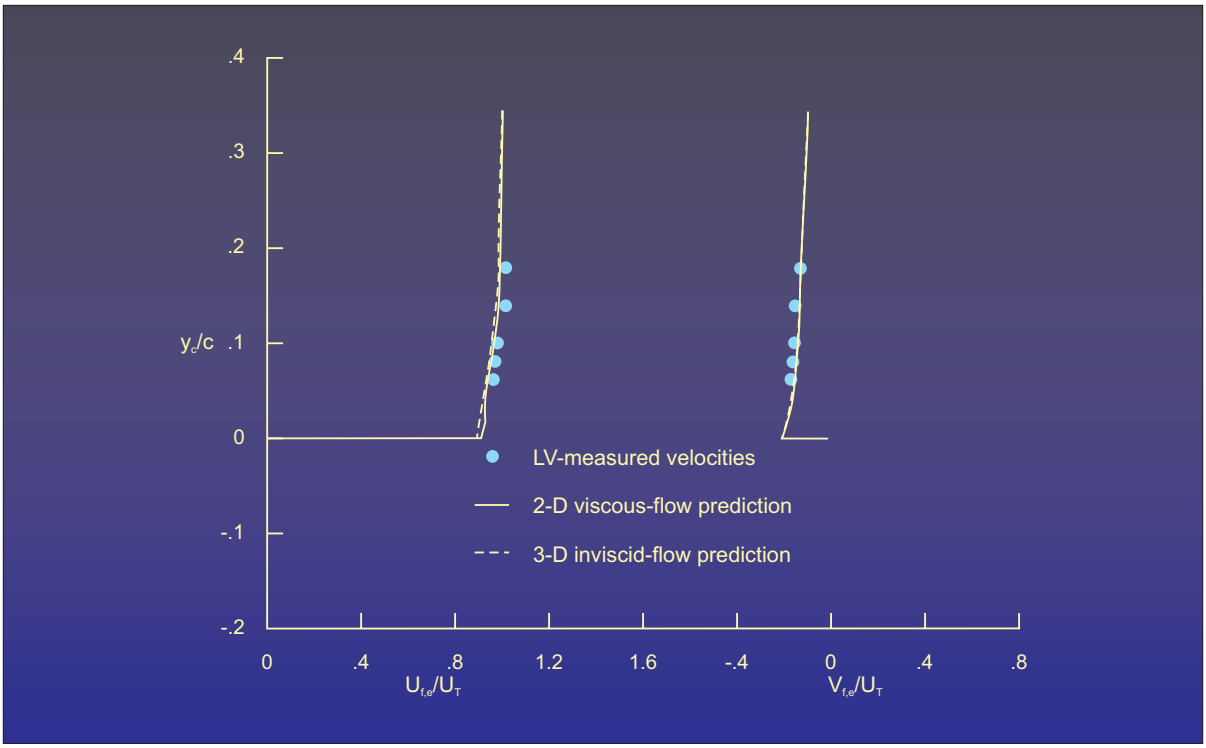

Figure 29.- Local velocity components along a scan perpendicular to wing chord at $x_c/c = 0.96$. $\alpha = 4.75°$.

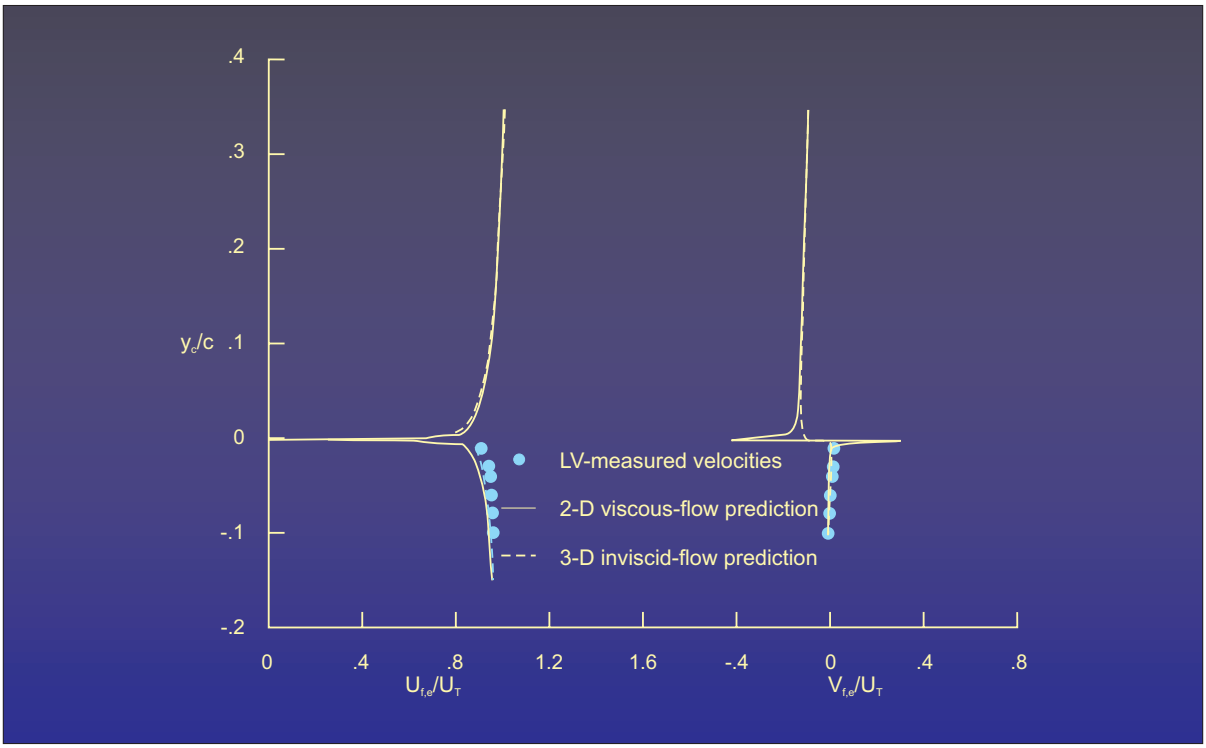

Figure 30.- Local velocity components along a scan perpendicular to wing chord at $x_c/c = 1.01$. $\alpha = 4.75°$.

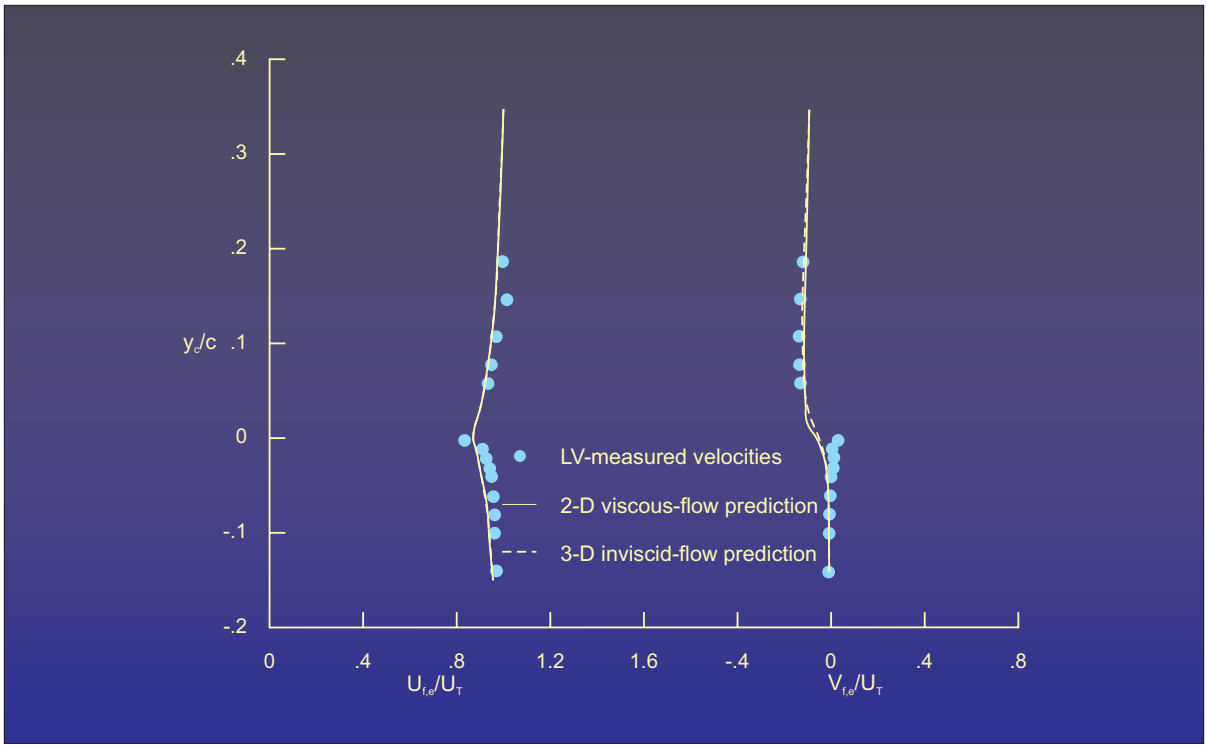

Figure 31.- Local velocity components along a scan perpendicular to wing chord at $x_c/c = 1.03$. $\alpha = 4.75°$.

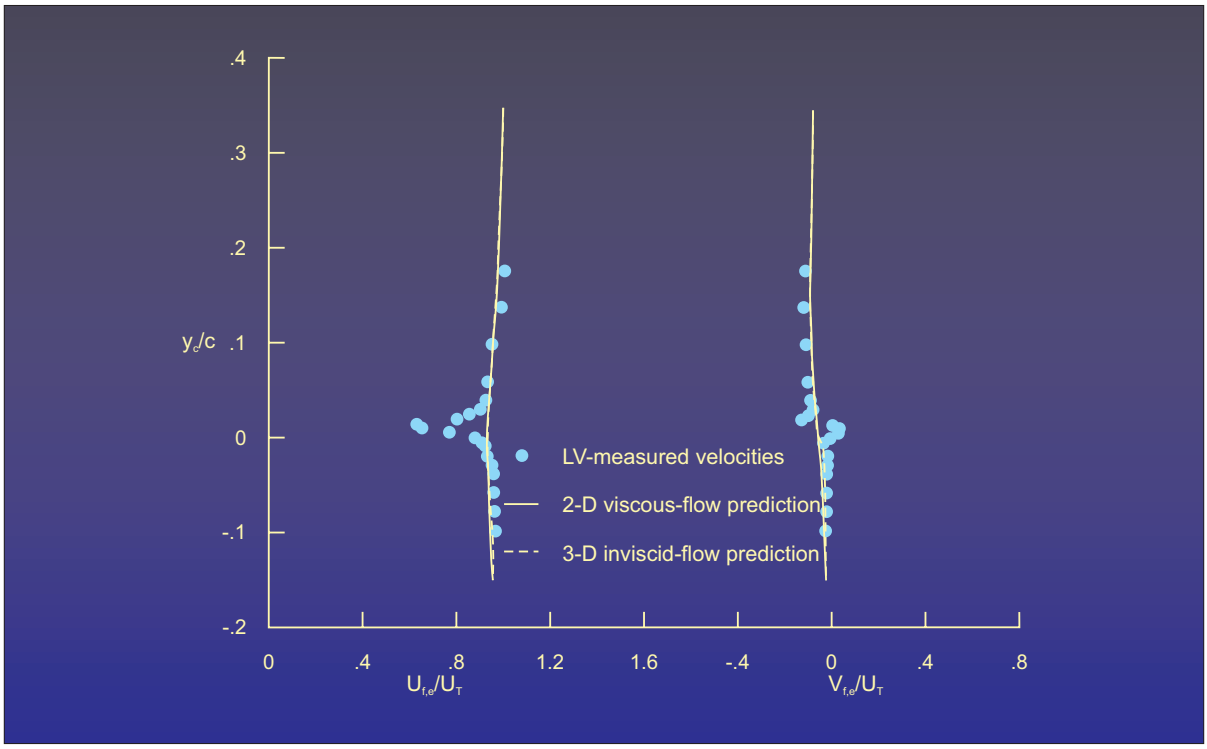

Figure 32.- Local velocity components along a scan perpendicular to wing chord at $x_c/c = 1.09$. $\alpha = 4.75°$.

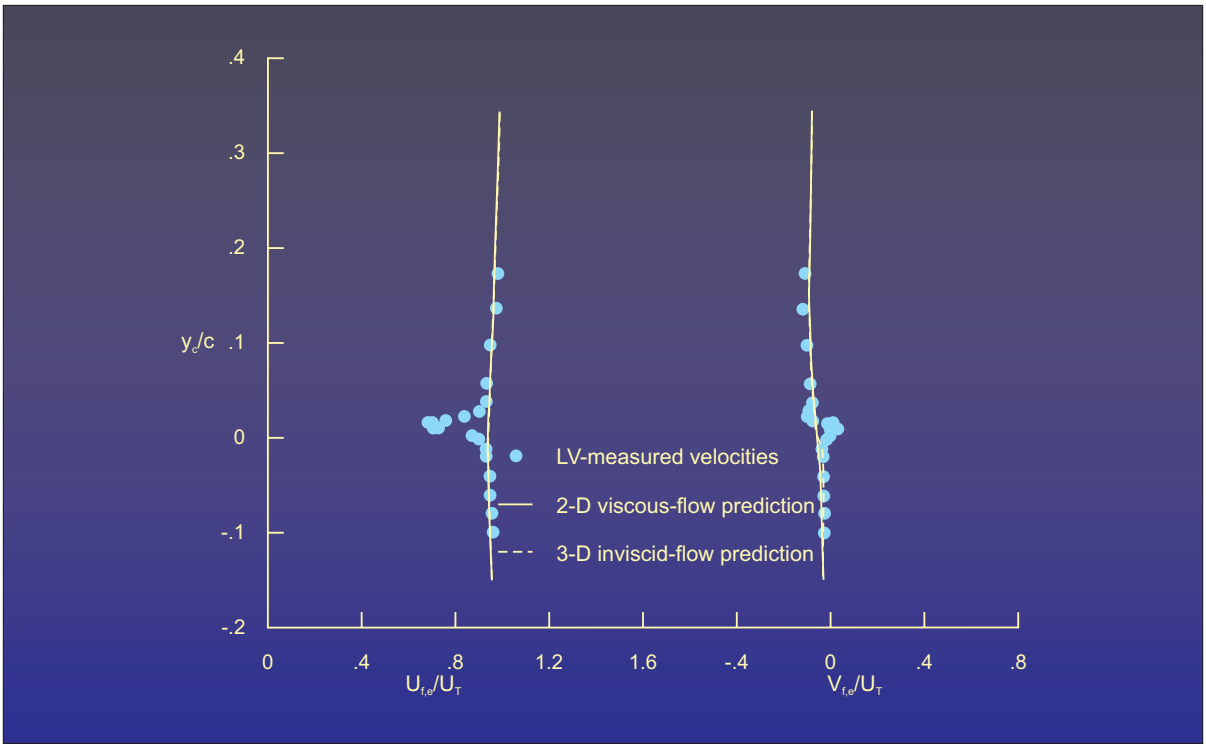

Figure 33.- Local velocity components along a scan perpendicular to wing chord at $x_c/c = 1.13$. $\alpha = 4.75°$.

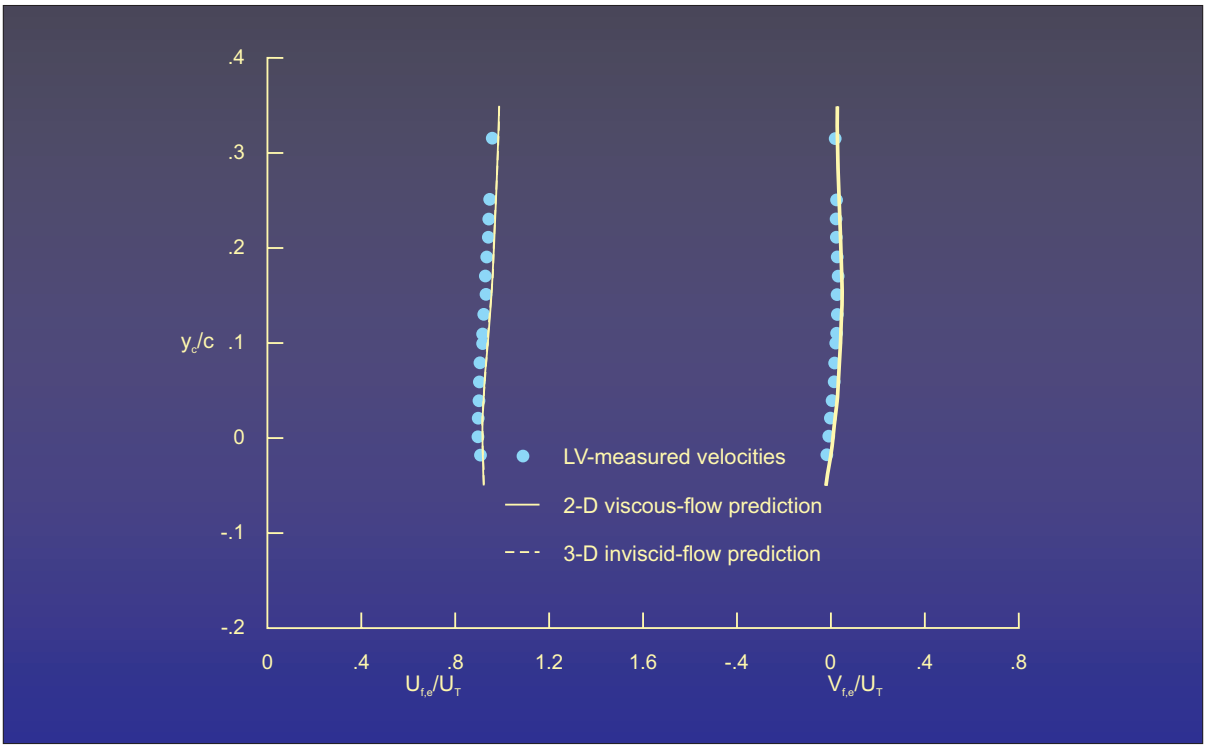

Figure 34.- Local velocity components along a scan perpendicular to wing chord at $x_c/c = -0.17$. $\alpha = 0.6°$.

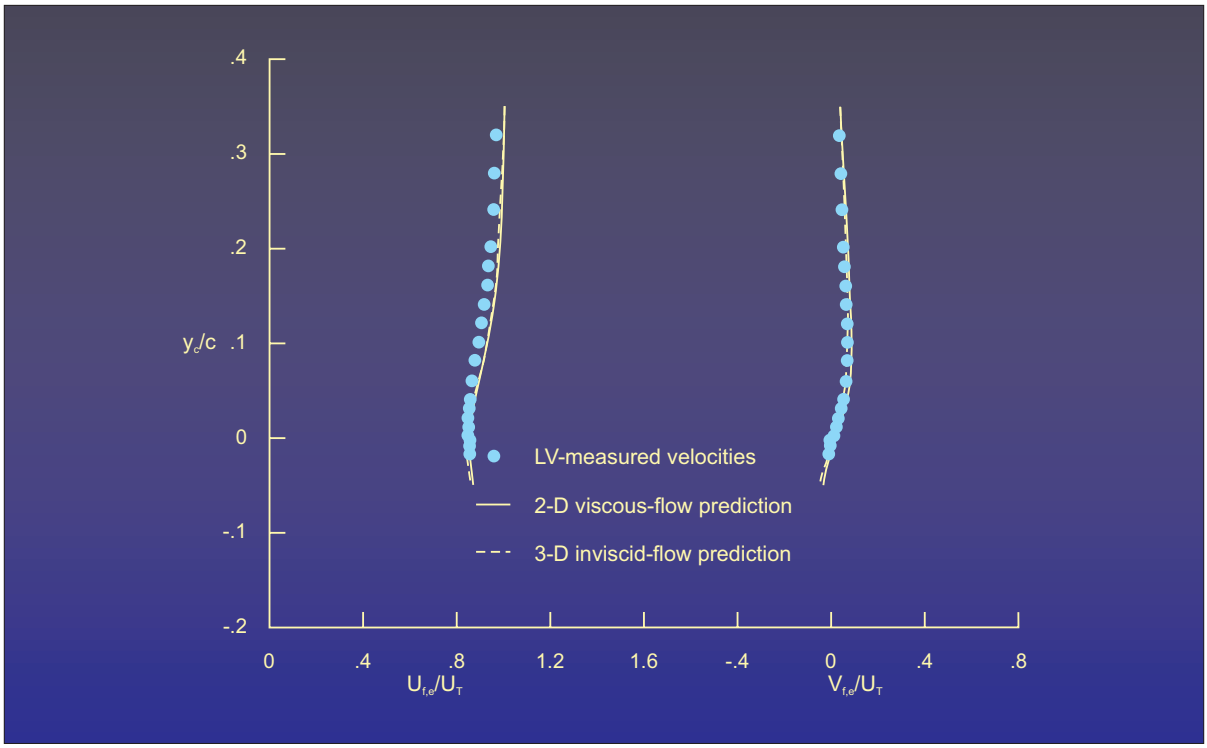

Figure 35.- Local velocity components along a scan perpendicular to wing chord at x_c/c = -0.09. $\alpha = 0.6^\circ$.

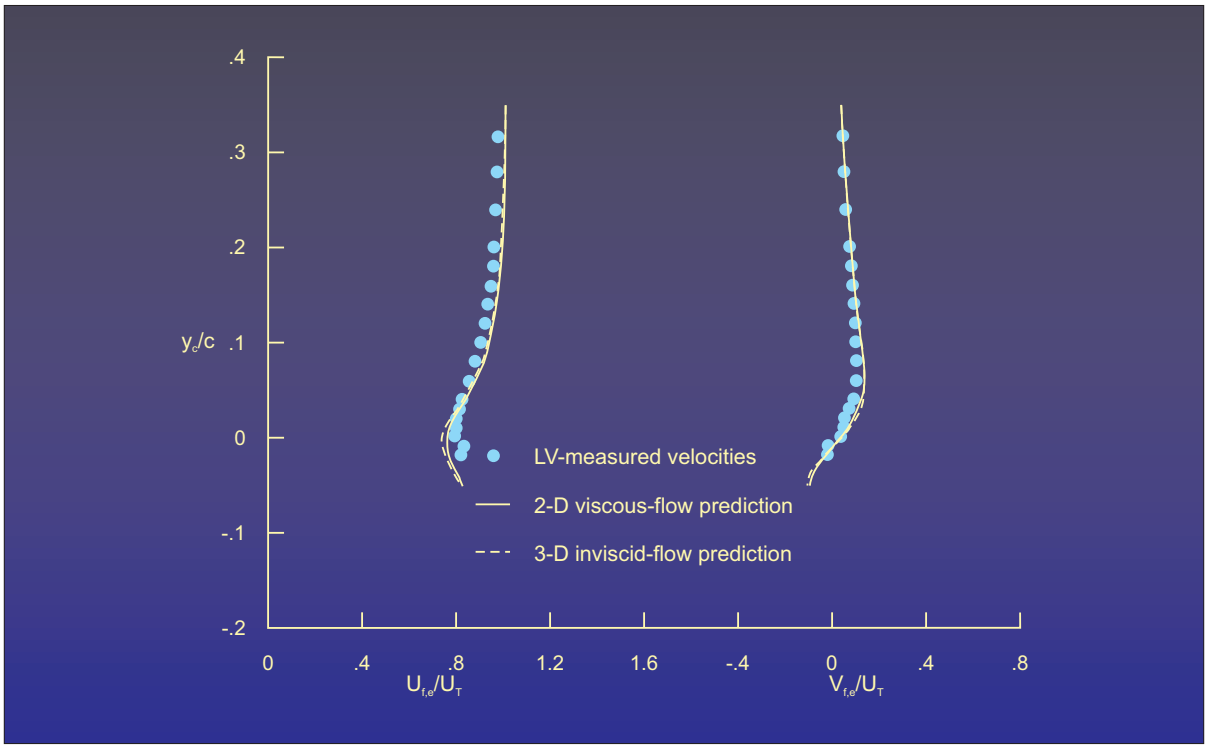

Figure 36.- Local velocity components along a scan perpendicular to wing chord at x_c/c = -0.05. $\alpha = 0.6^\circ$.

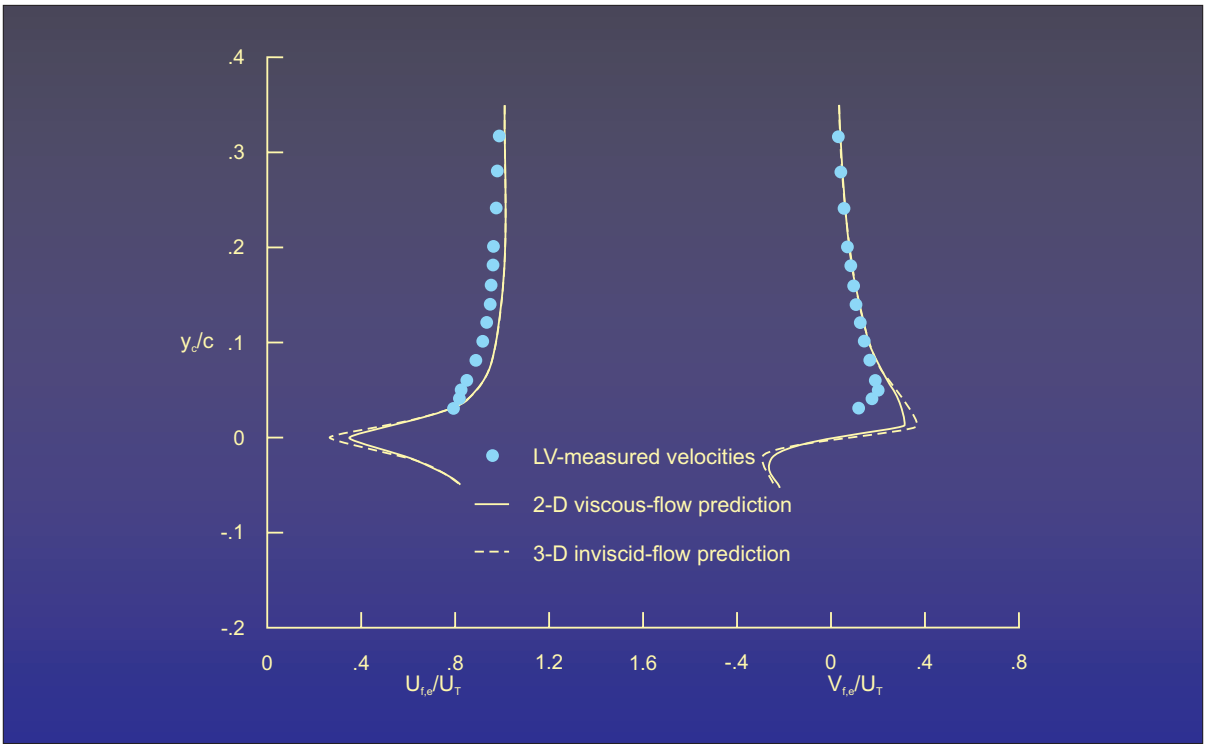

Figure 37.- Local velocity components along a scan perpendicular to wing chord at $x_c/c = 0$. $\alpha = 0.6°$.

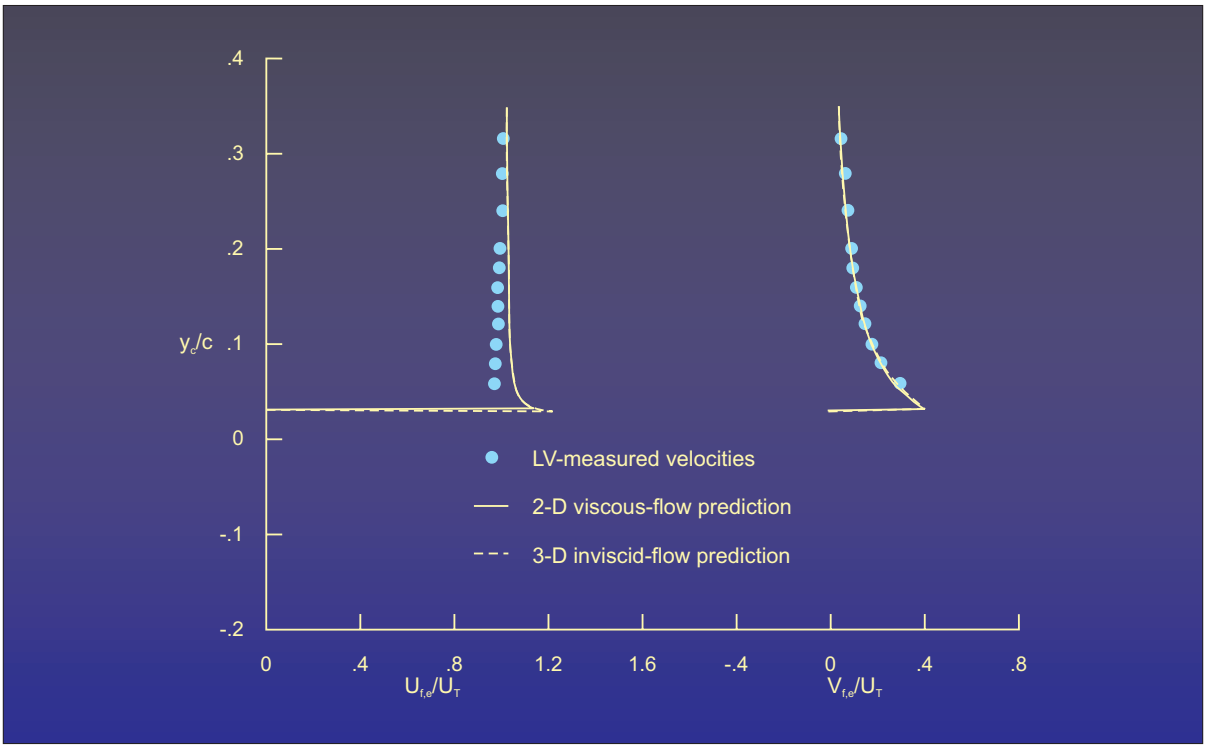

Figure 38.- Local velocity components along a scan perpendicular to wing chord at $x_c/c = 0.04$. $\alpha = 0.6°$.

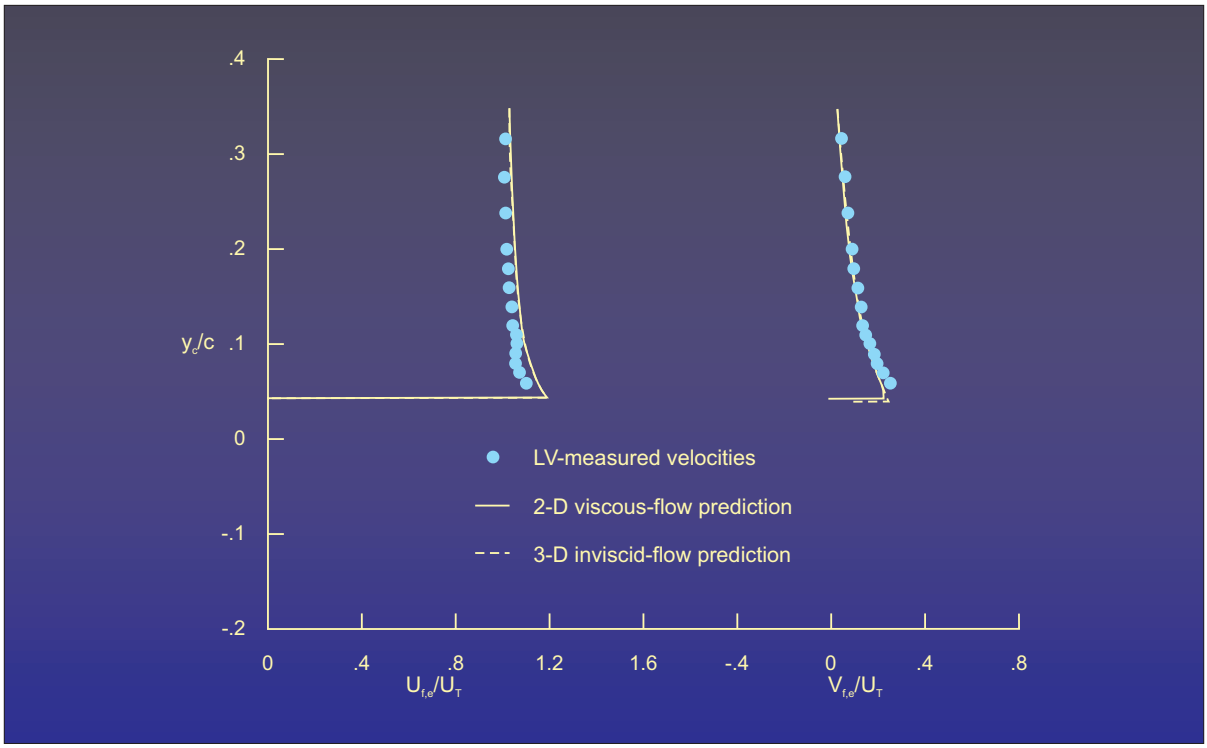

Figure 39.- Local velocity components along a scan perpendicular to wing chord at $x_c/c = 0.08$. $\alpha = 0.6°$.

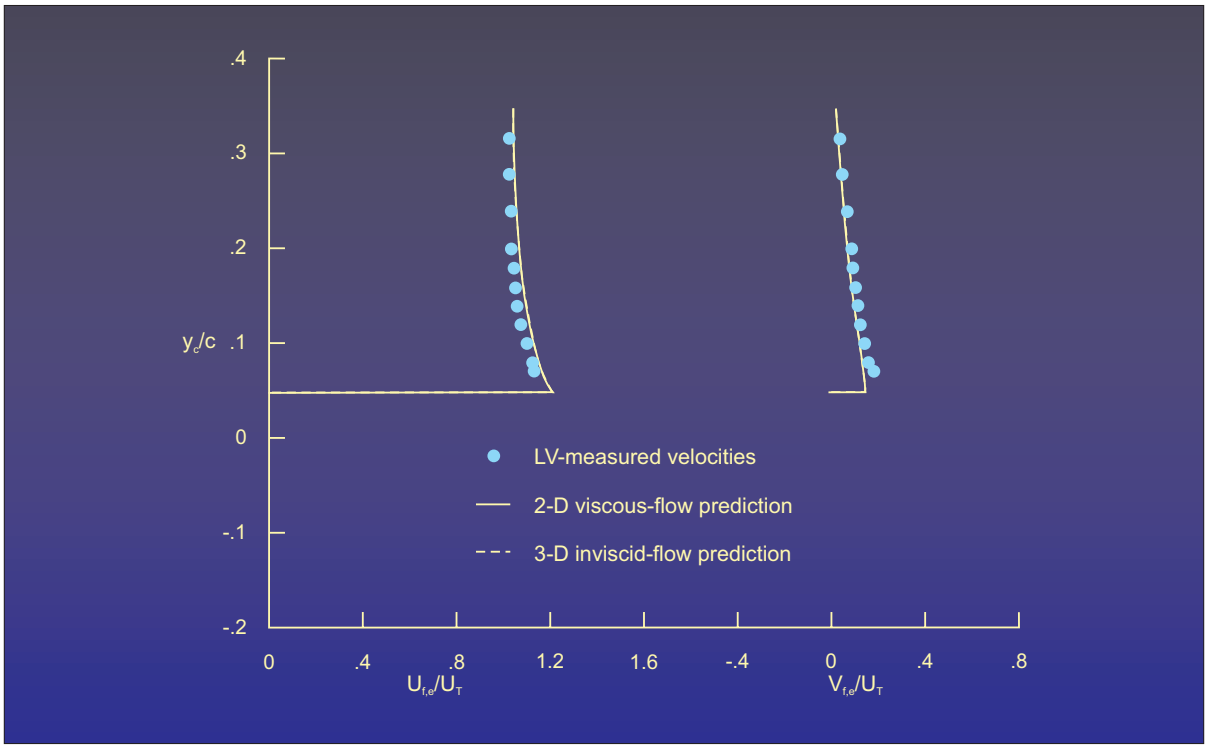

Figure 40.- Local velocity components along a scan perpendicular to wing chord at $x_c/c = 0.12$. $\alpha = 0.6°$.

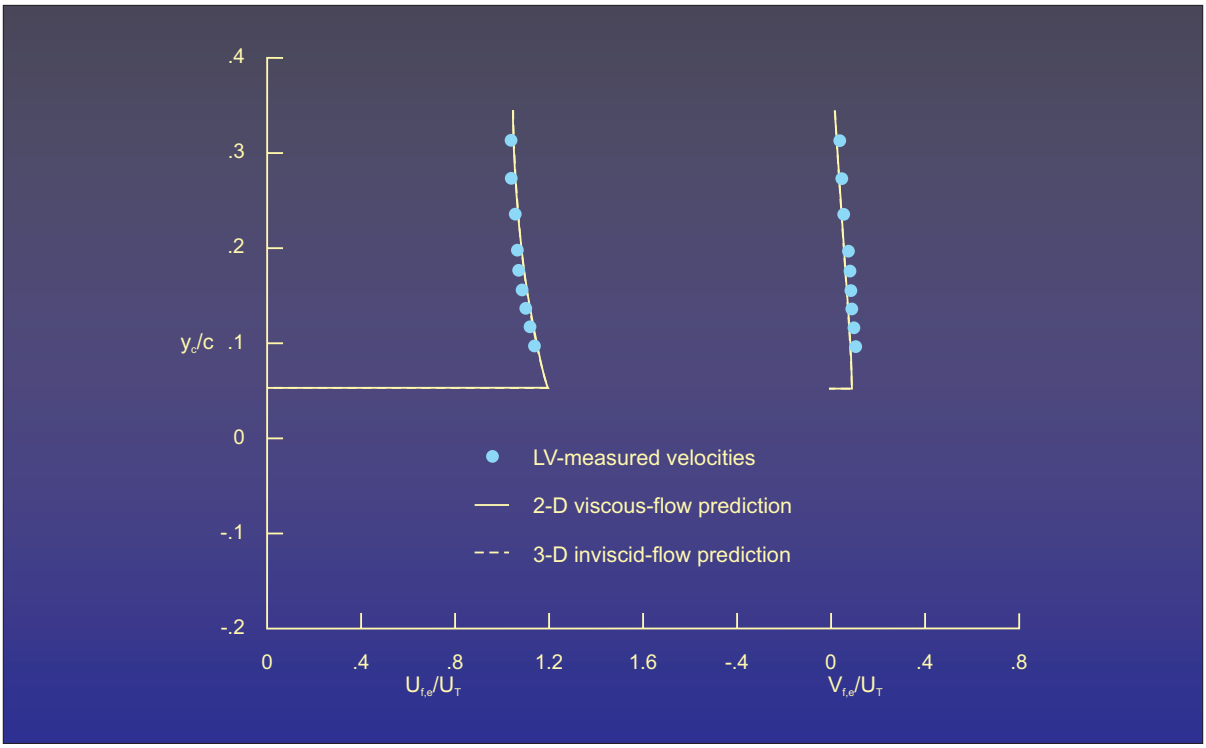

Figure 41.- Local velocity components along a scan perpendicular to wing chord at $x_c/c = 0.16$. $\alpha = 0.6^\circ$.

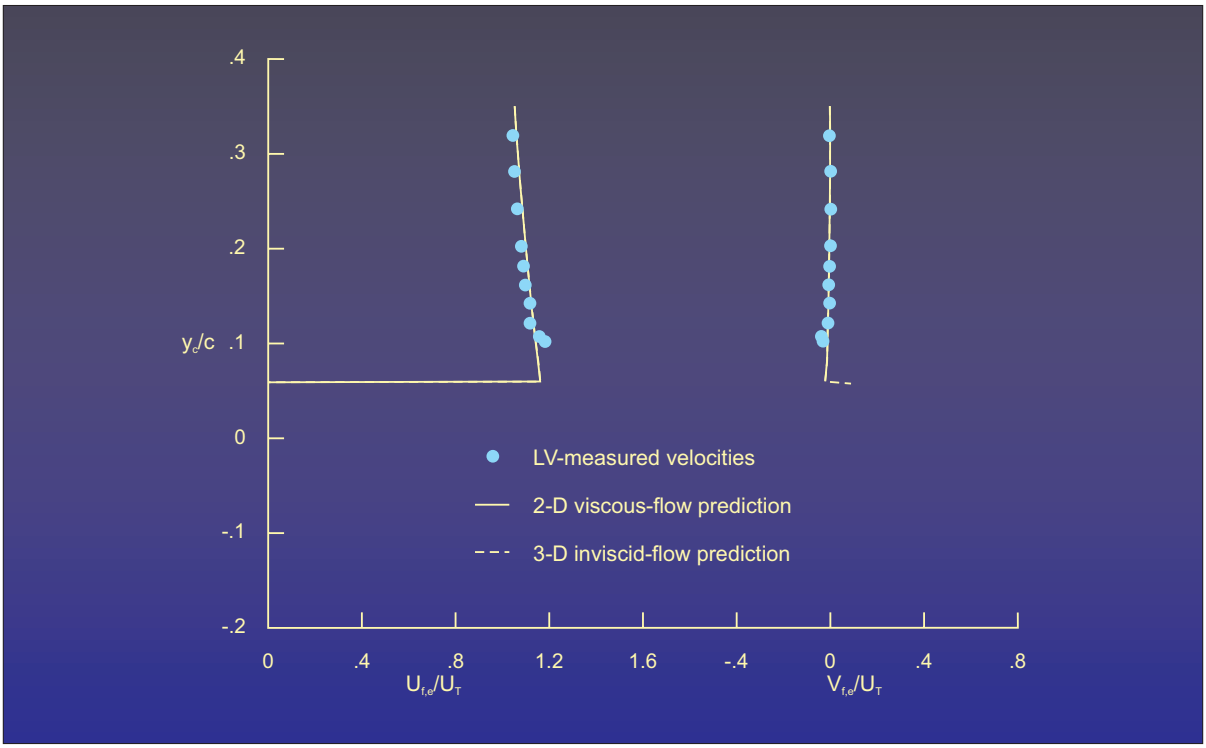

Figure 42.- Local velocity components along a scan perpendicular to wing chord at $x_c/c = 0.29$. $\alpha = 0.6^\circ$.

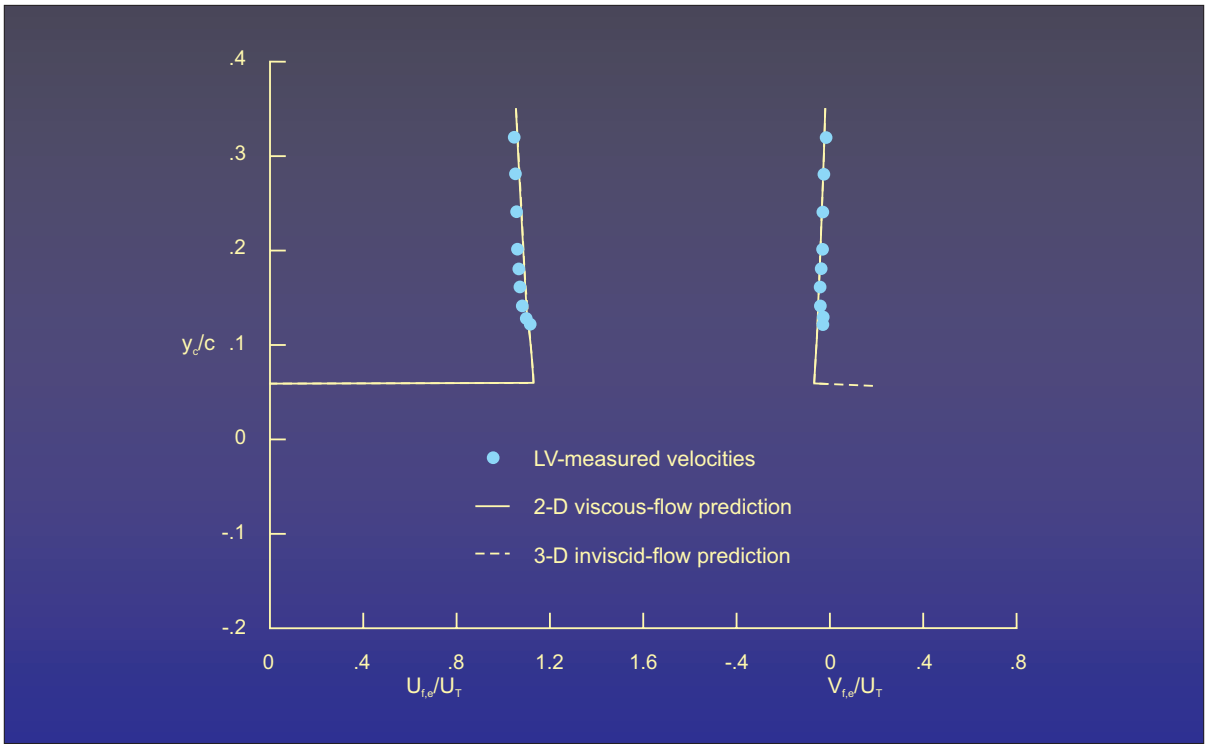

Figure 43.- Local velocity components along a scan perpendicular to wing chord at $x_c/c = 0.41$. $\alpha = 0.6°$.

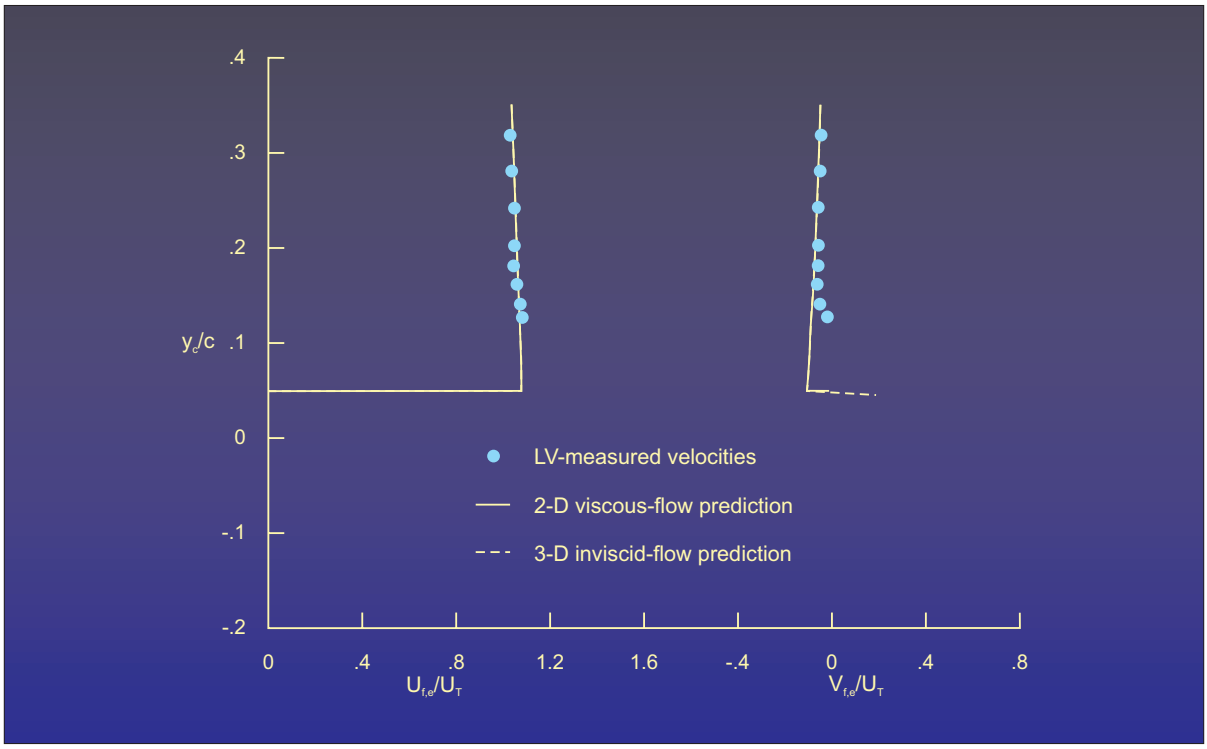

Figure 44.- Local velocity components along a scan perpendicular to wing chord at $x_c/c = 0.58$. $\alpha = 0.6°$.

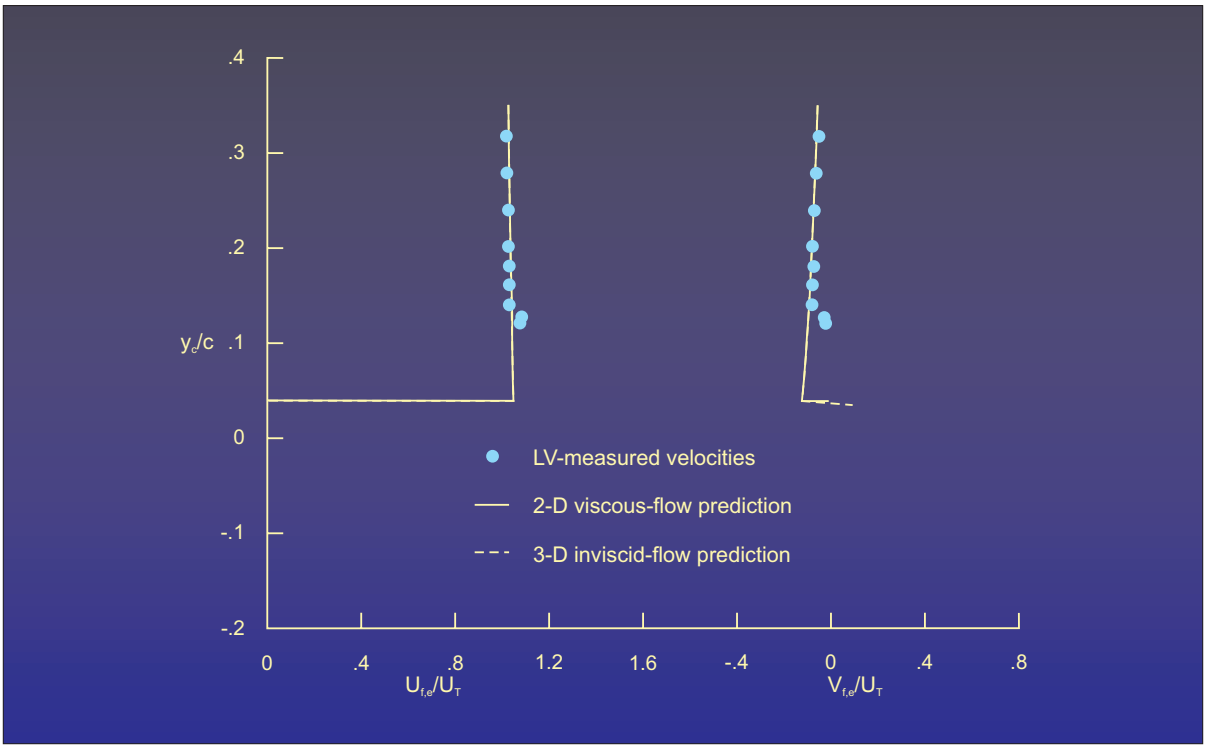

Figure 45.- Local velocity components along a scan perpendicular to wing chord at $x_c/c = 0.70$. $\alpha = 0.6^{\circ}$.

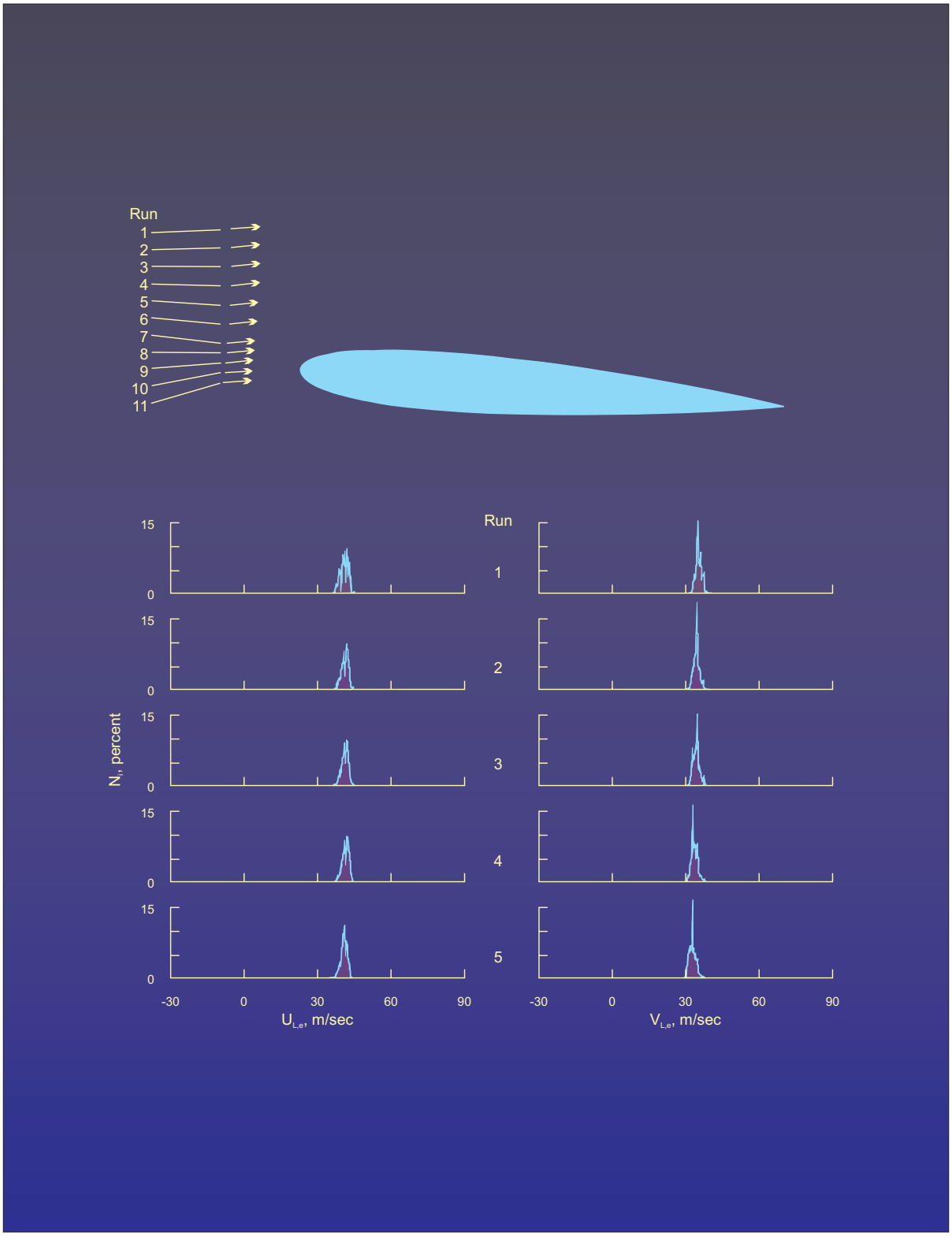

Figure 46.- Histograms in scan at x_c/c = -0.16. α = 4.75°.

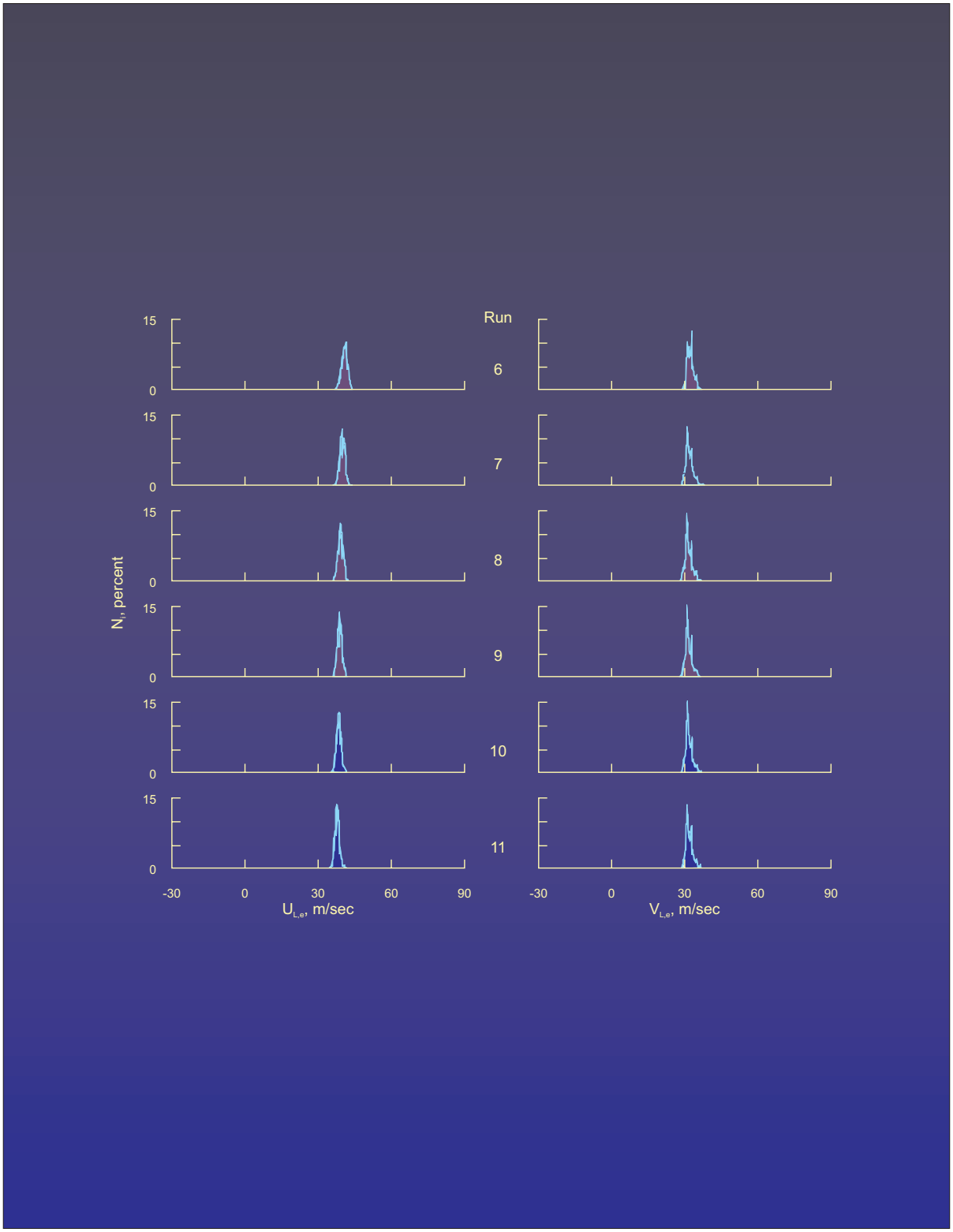

Figure 46.- Concluded.

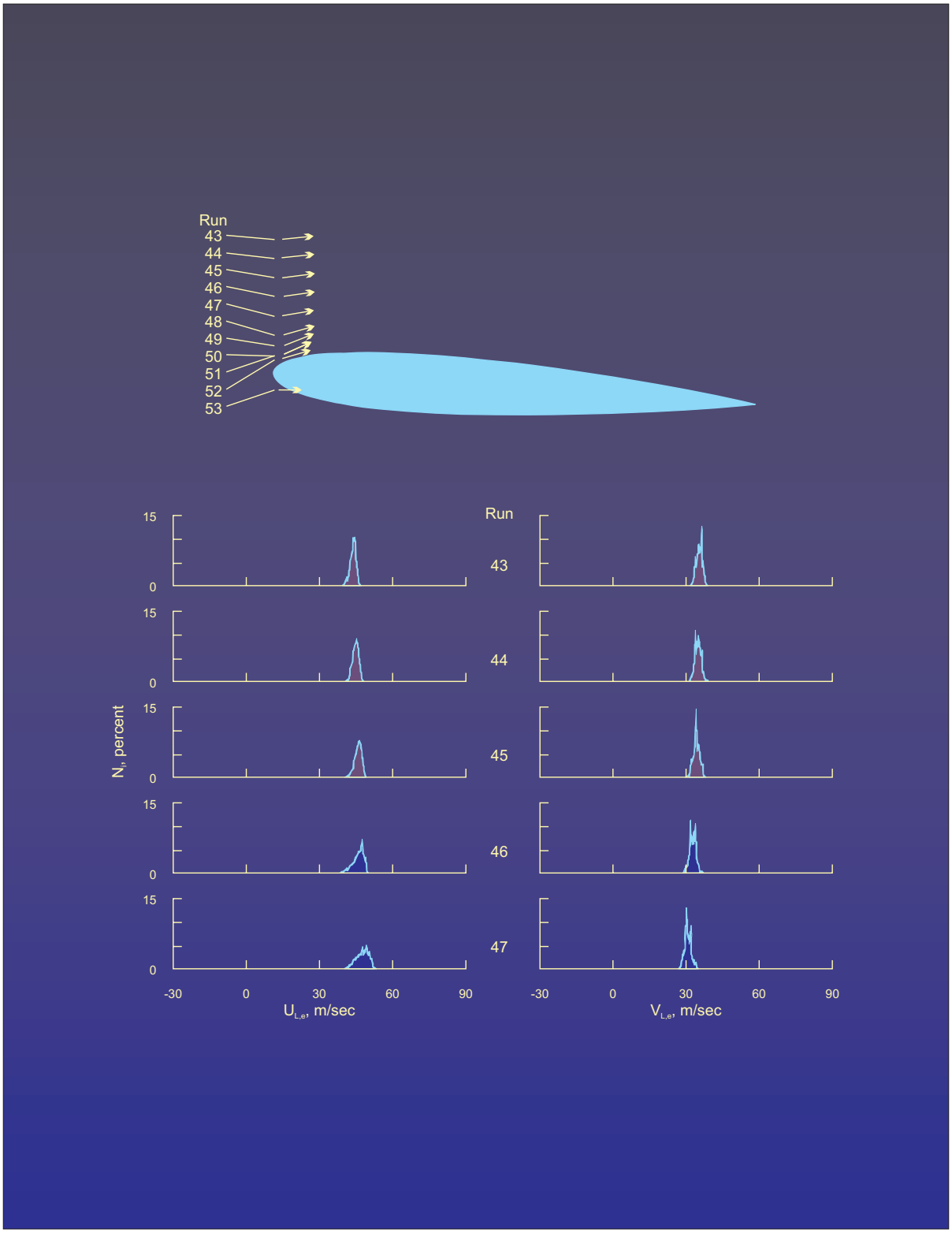

Figure 47.- Histograms in scan at $x_c/c = 0$. $\alpha = 4.75°$.

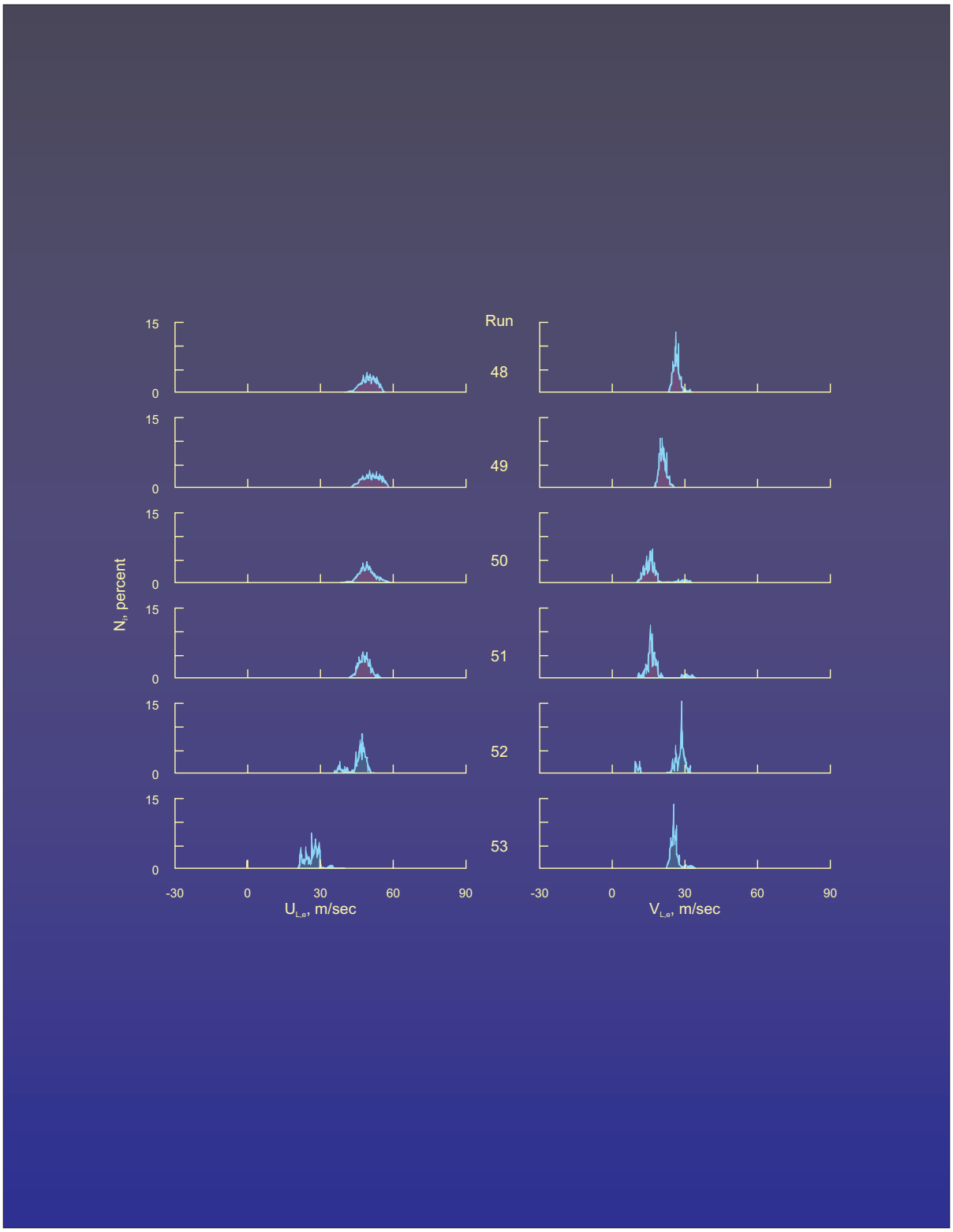

Figure 47.- Concluded.

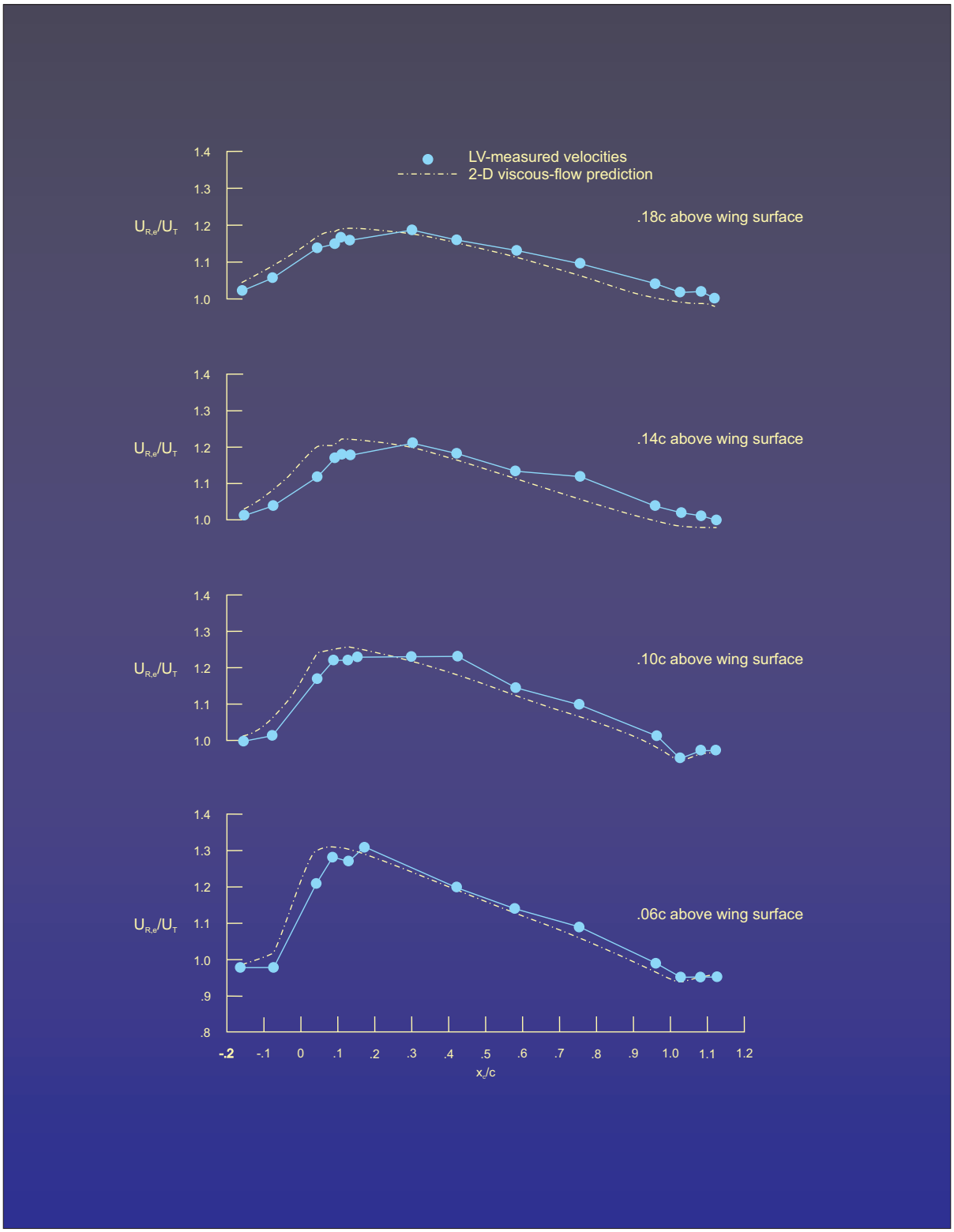

Figure 48.- Local total velocity comparison with theory at constant heights above wing. $\alpha = 4.75^{\circ}$.